Biophysical Journal Volume 70 April 1996 1643–1661

Molecular Dynamics Simulations of Water within Models of Ion Channels

J. Breed, R. Sankararamakrishnan, I. D. Kerr, and M. S. P. Sansom
Laboratory of Molecular Biophysics, The Rex Richards Building, University of Oxford, South Parks Road, Oxford OX1 3QU England

ABSTRACT The transbilayer pores formed by ion channel proteins contain extended columns of water molecules. The dynamic properties of such waters have been suggested to differ from those of water in its bulk state. Molecular dynamics simulations of ion channel models solvated within and at the mouths of their pores are used to investigate the dynamics and structure of intra-pore water. Three classes of channel model are investigated: a) parallel bundles of hydrophobic (Ala_{20}) α-helices; b) eight-stranded hydrophobic (Ala_{10}) antiparallel β-barrels; and c) parallel bundles of amphipathic α-helices (namely, δ-toxin, alamethicin, and nicotinic acetylcholine receptor M2 helix). The self-diffusion coefficients of water molecules within the pores are reduced significantly relative to bulk water in all of the models. Water rotational reorientation rates are also reduced within the pores, particularly in those pores formed by α-helix bundles. In the narrowest pore (that of the Ala_{20} pentameric helix bundle) self-diffusion coefficients and reorientation rates of intra-pore waters are reduced by approximately an order of magnitude relative to bulk solvent. In Ala_{20} helix bundles the water dipoles orient antiparallel to the helix dipoles. Such dipole/dipole interaction between water and pore may explain how water-filled ion channels may be formed by hydrophobic helices. In the bundles of amphipathic helices the orientation of water dipoles is modulated by the presence of charged side chains. No preferential orientation of water dipoles relative to the pore axis is observed in the hydrophobic β-barrel models.

INTRODUCTION

Bilayer-spanning pores are present in several classes of membrane transport protein: ion channels (Unwin, 1989; Hille, 1992), bacterial porins (Cowan et al., 1992), and aquaporins (Engel et al., 1994). All of these integral membrane proteins are thought to have a central pore that contains water molecules (Kreusch and Schulz, 1994; Unwin, 1995). To understand the molecular mechanisms of transport through such pores it is valuable to characterize the physical properties of intra-pore water (Dani and Levitt, 1990; Karshikoff et al., 1994). In particular, the dynamic behavior of intra-pore water will, alongside long-range interactions, influence the local dielectric constant and hence the strength of the electrostatic field experienced within the pore. Thus the dynamic behavior of intra-pore water may be expected to play an important role in the processes of ion permeation and/or gating of ion channels (Green and Lewis, 1991).

There have been numerous studies, both experimental and computational, of the behavior of water molecules interacting with the surfaces of globular proteins (reviews by Teeter, 1991; Daggett and Levitt, 1993). From such investigations it is evident that a degree of immobilization of water molecules occurs at the surface of a protein molecule. Rather less is known concerning the structure and dynamics of water within transbilayer channels. Studies of gramicidin A, a simple model channel containing a single-file column of waters, suggest that intra-pore water differs in its dynamic properties from bulk water (Chiu et al., 1991, 1993; Sancho et al., 1995). More generally, a number of experimental and computational studies (Granick, 1991) indicate that liquids confined within volumes of molecular dimensions exhibit perturbed structural and dynamic behavior. Using molecular dynamics (MD) simulations we have explored how water molecules behave when confined in channel-like hydrophobic cavities (Sansom et al., 1996). These and other studies demonstrate the need for a more detailed characterization to be made of the dynamic behavior of water molecules confined within realistic models of transbilayer pores. This is reinforced by experimental studies on the anion-selective porin PhoE, which show that water within the transbilayer pore differs in its physicochemical properties from bulk water (Gutman et al., 1992).

In this paper we examine two classes of ion channel model: a) channels formed by simple hydrophobic α-helix bundles (Kerr et al., 1994) and β-barrels (Sansom and Kerr, 1995); and b) channels formed by bundles of amphipathic α-helices (Sansom, 1991). These models are solvated within their pores and used as the basis of ~100-ps simulations of the dynamics of intra-pore water molecules. The simulations are analyzed in terms of the mobility of the water molecules and of their dipole orientations relative to the pore axis. The results suggest features of the perturbation of water dynamics that are common to different ion channel models. In particular, it seems that within protein pores water molecules are significantly immobilized, and that in many cases the water dipoles are preferentially aligned relative to the pore axis.

Received for publication 26 October 1995 and in final form 19 January 1996.

Address reprint requests to Dr. Mark S. P. Sansom, Laboratory of Molecular Biophysics, University of Oxford, The Rex Richards Building, South Parks Road, Oxford OX1 3QU England. Tel.: +44-1-865-275-371; Fax: +44-1-865-510-454; E-mail: mark@biop.ox.ac.uk.

Dr. Sankararamakrishnan's present address is Department of Physiology and Biophysics, Beckman Institute, University of Illinois at Urbana-Champaign, Urbana, IL 61801.

0006-3495/96/04/1643/19 $2.00

METHODS

General

Simulations were performed using CHARMM (Brooks et al., 1983) version 23f3 (for all models except M2α7N5; see Table 1) or XPLOR (Brünger, 1992) version 3.1 (for model M2α7N5) run on a DEC2100. All other calculations were carried out on Silicon Graphics R3000 and R4000 workstations. Structure diagrams were drawn using Molscript (Kraulis, 1991).

Solvation of initial models

Initial models of pores were generated using simulated annealing via restrained molecular dynamics (SA/MD), as described in previous publications (Kerr et al., 1994; Sansom and Kerr, 1995). Details of individual models are provided below. Extended atoms were used, i.e., only polar hydrogen atoms were explicitly represented.

The water model employed was a TIP3P three-site model (Jorgensen et al., 1983) with partial charges $q_O = -0.834$ and $q_H = +0.417$, modified as in the PARAM19 parameter set of CHARMM to allow internal flexibility of the water molecules. Model pores that were solvated used pre-equilibrated boxes of water molecules (see below for details). Water molecules were selected so that the central pore and the cap regions at either mouth of the pore were solvated, but such that no water molecules were present on the bilayer-exposed faces of the pores.

Models of pores

The models of transbilayer pores in this study were generated by SA/MD. This method has been described in detail in previous papers, as have the geometry and energetics of simple models of channels formed by purely hydrophobic (Ala_N) sequences (Kerr et al., 1994; Sansom and Kerr, 1995). The same method has also been used to model pores formed by parallel bundles of amphipathic α-helices, as are believed to be formed by many channel-forming peptides (CFPs) (Sansom, 1991), including δ-toxin (Kerr et al., 1996), alamethicin (Sansom, 1993), and synthetic peptides corresponding to the M2 helix of the nicotinic acetylcholine receptor (Montal, 1995). These various channel models are summarized in Table 1 and more detailed descriptions are provided in the following sections.

Simple hydrophobic pores

These models were generated from assemblies of peptide chains with the general sequence Ac-Ala_M-NH_2, in which the N-terminal acetyl group and the C-terminal amide group mimic the presence of preceding and following peptide bonds in an intact channel protein. By employing Ala_M sequences one may focus on the effects of confining water molecules within a protein pore and of water/backbone interactions, independent of possible interactions of water molecules with specific side chains. Furthermore, one should note that several examples of transbilayer pores formed by hydrophobic sequences are known: i) polyalanine and polyleucine adopt largely α-helical conformations and form H^+ channels in lipid bilayers (Oliver and Deamer, 1994); ii) the hydrophobic α-helical peptide Boc-(Ala-Aib-Ala-Aib-Ala)$_4$OMe forms voltage-gated channels (Menestrina et al., 1986); and iii) the pore-lining α-helices of phospholamban are almost entirely hydrophobic (Arkin et al., 1994, 1995; Adams et al., 1995). Thus, simulations of water within hydrophobic transbilayer pores are of direct relevance to these systems.

Two classes of model of hydrophobic pores have been considered. A recurrent motif in many channels is a bundle of approximately parallel α-helices surrounding a central pore (Oiki et al., 1990). For example, a pentameric helix bundle lines the pore of the nicotinic acetylcholine receptor, and hexameric helix bundles are formed by several channel-forming peptides (see below). As a first approximation to such structures pores formed by parallel bundles of Ala_{20} helices were modeled (Kerr et al., 1994). Both pentameric (AN5; Table 1) and hexameric (AN6) bundles have been investigated. In models AN5 and AN6 the helices exhibit ridges-in-grooves packing, forming left-handed coiled coils around a central water-filled pore.

Not all transbilayer pores are formed by α-helices. In porins a 16-strand (18-strand in maltoporin; Schirmer et al., 1995) antiparallel β-barrel surrounds a central channel (Cowan et al., 1992). Furthermore, an 8-strand antiparallel β-barrel has been widely invoked as a possible structure for the pore domain of K^+ and related voltage-gated channels (Bogusz et al., 1992). In the context of the latter, we have investigated model pores formed by antiparallel β-barrels of eight Ala_{10} strands (Sansom and Kerr, 1995). Models BN8S8 and BN8S12 (Table 1) have the same number of strands but differ in the stagger of their strands relative to one another (as specified by the shear number S). Thus BN8S12, having the larger shear number, forms a somewhat wider and shorter pore than does BN8S8.

Amphipathic α-helix bundles

Some of the simplest ion channels are those formed by parallel bundles of amphipathic helices (Sansom, 1991). These include channel-forming peptides (CFPs) such as δ-toxin (Mellor et al., 1988; Kerr et al., 1995) and alamethicin (Sansom, 1993), and synthetic peptide fragments derived from more complex ion channel proteins, such as the M2δ peptide derived from *Torpedo* nAChR (Montal, 1995).

δ-Toxin is a 26-residue CFP from *Staphylococcus aureus* that has been intensively studied, both in terms of its physico-chemical and its channel-forming properties. NMR studies (Tappin et al., 1988) indicate that δ-toxin forms highly amphipathic helices. The concentration and voltage dependence of channel formation suggest that on average six δ-toxin helices self-assemble within the lipid bilayer to form a parallel helix bundle (Mellor et al., 1988). Models of hexameric δ-toxin bundles, in which the polar faces of the helices form the pore lining, whereas the hydrophobic faces point outward toward the surrounding lipid, have been generated using SA/MD (Kerr et al., 1996). The helices are packed so as to form a left-handed coiled coil, as is the case for AN5 and AN6.

Alamethicin (Alm) is the most intensively studied example of an ion channel based on the helix bundle motif (Sansom, 1993). It is a 20-residue

TABLE 1 Model pores

Model	Sequence	Pore structure
AN5	Ac-$(A)_{20}$-NH_2	N = 5 parallel α-helix bundle
AN6	Ac-$(A)_{20}$-NH_2	N = 6 parallel α-helix bundle
BN8S8	Ac-$(A)_{10}$-NH_2	N = 8, S = 8 antiparallel β-barrel
BN8S12	Ac-$(A)_{10}$-NH_2	N = 8, S = 12 antiparallel β-barrel
δ-ToxN6	f-M-A-*Q*-*D*-I-I-*S*-*T*-I-G-*D*-L-V-*K*-W-I-I-*D*-*T*-V-*N*-*K*-F-*T*-*K*-*K*	N = 6 parallel α-helix bundle
AlmN6	Ac-U-P-U-A-U-A-Q-U-V-U-G-L-U-P-V-U-U-*E*-Q-F-OH	N = 6 parallel α-helix bundle
AlmN8	Ac-U-P-U-A-U-A-Q-U-V-U-G-L-U-P-V-U-U-*E*-Q-F-OH	N = 8 parallel α-helix bundle
M2α7N5	Ac-*E*-*K*-I-*S*-L-G-I-*T*-V-L-L-*S*-L-*T*-V-F-M-L-L-V-A-*E*-NH_2	N = 5 parallel α-helix bundle

peptaibol, a member of a family of CFPs that have a high content of the helicogenic amino acid α-aminoisobutyric acid (Aib). Both x-ray (Fox and Richards, 1982) and NMR (Esposito et al., 1987) studies demonstrate that Alm forms an α-helix, kinked in its center by Pro-14. Channels are formed by assemblies of between four and 12 alamethicin monomers. We have used SA/MD to model pores formed by bundles of five to nine Alm monomers (Sansom, 1993; Breed and Sansom, 1994). In these bundles the N-terminal segments of the helices are close packed, whereas the C-terminal segments are splayed outward so as to form a wider channel mouth at the C-terminus. Models AlmN6 and AlmN8 allow us to explore water dynamics in two pores of similar shape but differing radii.

Sequence M2α7 corresponds to the channel-lining M2 helix of the neuronal α7 nAChR. M2α7 is similar to M2δ, a synthetic peptide that has been shown to adopt a transbilayer α-helical conformation and which forms ion channels that resemble those of the parent nAChR (Montal, 1995). In the intact nAChR the pore is formed by a pentameric assembly of approximately parallel M2 helices (Unwin, 1995). In model M2α7N5 five helices are packed in an approximately parallel fashion, such that the C-terminal mouth is somewhat wider than the N-terminal mouth (Sankararamakrishnan and Sansom, 1995a). This is similar to the case in the Alm models, in that it allows the uncompensated negative charges of the Glu-22 side chains to be spaced further apart.

Overall, δ-ToxN6, AlmN6, AlmN8, and M2α7N5 provide a range of different models of pores formed by amphipathic helix bundles. δ-ToxN6 and M2α7N5 contain linear helices and have highly polar channel linings, whereas AlmN6 and AlmN8 have less polar linings to their pores, and their constituent helices are kinked by proline residues. Thus these models permit exploration of water dynamics in pores of differing geometry and polarity.

MD simulations

Solvated model pores were energy minimized before MD simulations. For all models except M2α7N5 a four-stage energy minimization was performed: a) 1000 cycles of adopted basis Newton Raphson (ABNR) minimization with the protein atoms fixed; b) 1000 cycles of ABNR with the protein backbone atoms restrained; c) 1000 cycles of ABNR with weak restraints on the protein Cα atoms only; and d) 1000 cycles of ABNR with no positional restraints. For M2α7N5 the system was minimized until the norm of the energy gradient was less than 0.01. Note that during some energy minimizations and MD simulations restraints were applied to water and/or protein atoms. In some models (see below) protein atoms were restrained using inter-helix distance restraints (Kerr et al., 1994). In some models restraints were applied to water molecules to prevent them from evaporating from the ends of the pore. The form of the restraining potential, applied to the waters using the MMFP module of CHARMM, was

$$E = \frac{F}{2}\exp\left(-\frac{\Delta}{\lambda}\right) \qquad \text{if } \Delta > 0, \tag{1}$$

or

$$E = F\left[1 - \frac{1}{2}\exp\left(+\frac{\Delta}{\lambda}\right)\right] \qquad \text{if } \Delta \leq 0, \tag{2}$$

where $F = -7.5$ kcal/mol and $\lambda = 0.25$ Å, and in which $\Delta = r - r_{WALL}$, i.e., the distance of the atom from the restraining "wall." Note that Eq. 1 applies to atoms outside the wall and Eq. 2 applies to atoms inside the wall. Further details of both classes of restraint are given below.

MD simulations used a 1-fs time step. For all models other than M2α7N5 the system was heated from 0 to 300 K in 6 ps (5-K, 0.1-ps steps) and equilibrated for 9 ps at 300 K by rescaling velocities every 0.1 ps. The production stage of the simulation generally was run for 85 ps (485 ps for AN5/500; 60 ps for AlmN6 and AlmN8), and dynamic properties of water were analyzed over the 170 coordinate set trajectories (485 coordinate sets for AN5/500; 120 coordinate sets for AlmN6 and AlmN8) saved during this latter stage of the simulations. Non-bonded interactions (both electrostatic and van der Waals) between distant atoms were truncated using a shift function (Brooks et al., 1983) with a cutoff of 13.0 Å. In simulation AN5/G a group cutoff was applied to electrostatic interactions, using a switching function and a cutoff distance of 13.0 Å.

For M2α7N5 MD simulations were performed essentially as described in Sankararamakrishnan and Sansom (1994). During the heating stage (3 ps) the temperature was increased from 0 to 300 K in steps of 50 K, and at each temperature 0.5 ps of MD simulation was run. Velocities were rescaled every 0.1 ps during heating, and every 1 ps during the equilibration period (22 ps). At the end of equilibration, a further 100 ps simulation was performed, with the system maintained at a constant temperature of 300 K by coupling to a temperature bath. A cutoff of 9.5 Å was used for non-bonded interactions.

Analysis

Three parameters characterizing the dynamic behavior of water molecules were estimated: the self-diffusion coefficient, D, and the rotational correlation times, τ_1 and τ_2. The self-diffusion coefficient for each water molecule was obtained by evaluation of its mean square displacement as a function of time:

$$\langle r(t)^2 \rangle = \langle (\mathbf{r}(t) - \mathbf{r}(0))^2 \rangle, \tag{3}$$

and using the relationship

$$\lim_{t \to \infty} \langle r(t)^2 \rangle = 6Dt + C \tag{4}$$

to fit the $\langle r(t)^2 \rangle$ data for $t = 3$ to 6 ps. Inspection of $\langle r(t)^2 \rangle$ vs. t curves for individual waters revealed them to approach linearity within this region, justifying the fitting of Eq. 4 to the data. Comparable relationships were used to estimate the components of the self-diffusion coefficient parallel to the longitudinal axis of the pore (D_Z) and in the plane perpendicular to the pore axis (D_{XY}). Rotational correlation functions were defined in terms of the angle, $\theta(t)$, made by the dipole of a water molecule at time 0 and the dipole of the same water molecule at time t. Two rotational correlation functions were estimated for each water molecule:

$$C_1(t) = \langle \cos(\theta(t)) \rangle \tag{5}$$

and

$$C_2(t) = \langle (3\cos^2\theta(t) - 1)/2 \rangle. \tag{6}$$

These were fitted (for the regions from 0.5 to 5.0 ps) as mono-exponential decays with time constants τ_1 and τ_2, respectively. Again, inspection of plots of $C_1(t)$ and $C_2(t)$ for individual waters supported the fitting of mono-exponentials to these regions. Rotational reorientation rates were calculated as the reciprocals of these time constants.

Water dipole orientations were analyzed from the final coordinate sets generated at the end of the simulations. The orientation of water molecules relative to the pore (z) axis was measured in terms of the projection onto the z axis of the dipole moment of each water, μ_Z. Note that for an ideal TIP3P water molecule with its dipole exactly parallel to the z axis, $\mu_Z = 2.35$ Debye. The pore/water interaction energy of the models was defined as $\Delta E_{PORE/WATER} = E(\text{pore} + \text{water}) - E(\text{pore}) - E(\text{water})$. The interaction energy between the protein segments making up the pore was defined as $\Delta E_{PROTEIN/PROTEIN} = E(\text{pore}) - E(\text{isolated TM segments})$. Pore radius profiles were measured using HOLE (Smart et al., 1993), which calculates the pore radius as a function of distance along the pore (z) axis.

RESULTS

Simulations AN5 and AN6

Models AN5 and AN6 consist of parallel bundles of hydrophobic helices surrounding a central pore of water molecules. Water molecules were added by taking a pre-equili-

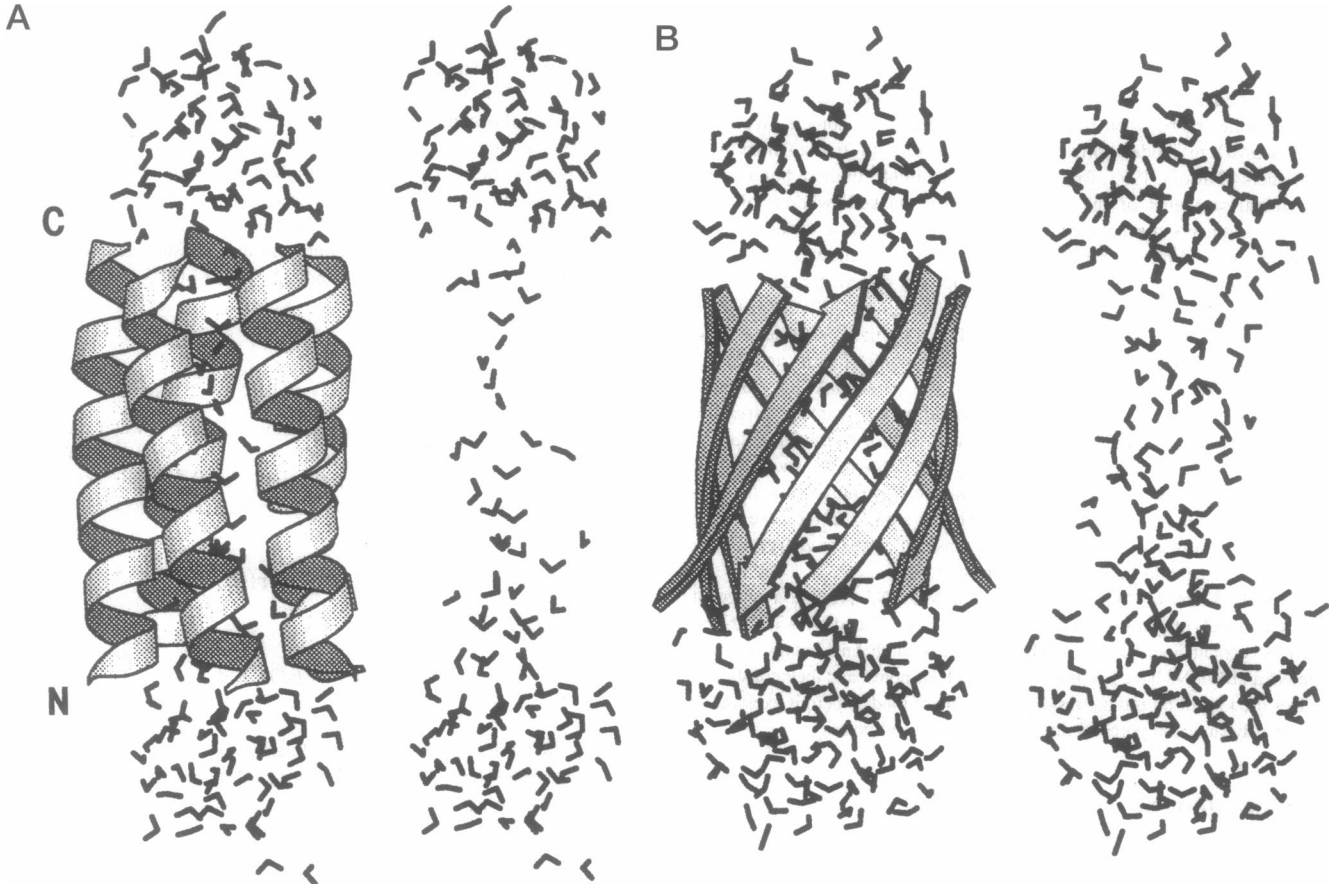

FIGURE 1 Ala_M model pores. Molscript (Kraulis, 1991) generated diagrams of the structures of models (*a*) AN5 and (*b*) BN8S8 at the end of 100 ps MD. In both cases the pore model is shown in ribbon format along with its water molecules on the left-hand side, and the water molecules alone are shown on the right-hand side.

brated cylinder (length, 60 Å; radius, 6.9 Å for AN5, 8.1 Å for AN6), and removing all water molecules closer than 1.6 Å to protein atoms plus those in the "pore" zone lying outside the helix bundle. To prevent water molecules from evaporating from the pore a restraining potential was applied to the waters. This comprised a cylindrical cavity, of length 60 Å and radius 8 Å (for AN5) or 9.1 Å (for AN6). Note that this restraining potential only came into play for waters at the mouths of the pore, as the cavity radius is greater than the van der Waals radius of the pore lining. A number of control simulations were also performed that explored the effects of restraints on the polypeptide backbone. These did not yield significantly different results in terms of water dynamics and orientations. In AN5 and AN6 such restraints were not applied to the protein backbone.

The structure of model AN5 and of its water at the end of the MD run are shown in Fig. 1 *a*. The left-handed coiled coil structure is retained. Indeed, in the initial model the mean helix/helix separation was $R = 7.8\ (\pm 0.1)$ Å, and the mean helix crossing angle was $\Omega = +11.7\ (\pm 0.5)°$, whereas after MD $R = 7.8\ (\pm 0.4)$ Å and $\Omega = +11.9\ (\pm 4.3)°$. Similarly, for AN6 before solvation $R = 7.8\ (\pm 0.2)$ Å and $\Omega = +11.6\ (\pm 2.4)°$, whereas after MD $R = 8.4\ (\pm 0.7)$ Å and $\Omega = +11.1\ (\pm 2.9)°$. Thus solvation and 100 ps of MD do not significantly alter the packing of the helices within these bundles, as confirmed by the relatively low Cα atom root mean square deviations (RMSDs) if one compares the beginning and end of the MD simulations (Table 2).

From Fig. 1 *a* it is evident that the AN5 pore is fairly narrow; in places it is only one or two water molecules wide. This is confirmed by the pore radius profile (Fig. 2 *a*), which reveals a pore of radius 2 to 2.5 Å and of length ~30 Å. The pore length is about the same for AN6, but the radius is increased to ~4 Å.

The energetics of protein/protein and pore/water interactions within the bundles at the end of the MD simulations are summarized in Table 2. Favorable interactions between the Ala_{20} helices are van der Waals in origin, with a small unfavorable electrostatic component reflecting helix dipole repulsions. From the pore/water interaction energies it can be seen that, despite the hydrophobic nature of the helices, there is a large favorable electrostatic term. This is a result of interaction of the water dipoles with the helix dipoles, as is demonstrated below.

TABLE 2 Model pores: energetics

Model	$\Delta E^{VDW}_{PORE/WATER}$ (kcal/mol)	$\Delta E^{ELEC}_{PORE/WATER}$ (kcal/mol)	$\Delta E^{VDW}_{PROTEIN/PROTEIN}$ (kcal/mol)	$\Delta E^{ELEC}_{PROTEIN/PROTEIN}$ (kcal/mol)	RMSD-Cα (Å)
AN5	−128	−477	−120	+46	1.6
AN5/G	−159	−440	−83	+26	3.0
AN6	−191	−606	−118	+49	2.1
BN8S8	−208	−369	−183	−291	2.8
BN8S12	−191	−342	−210	−274	1.7
δ-Toxin	−404	−4073	−263	−797	2.1
AlmN6	−352	−1590	−144	+46	2.4
AlmN8	−502	−2425	−201	+71	2.9
M2α7	−362	−2616	−82	−20	1.4

All energies refer to the model at the end of the MD simulation. $\Delta E^{VDW}_{PORE/WATER}$ and $\Delta E^{ELEC}_{PORE/WATER}$ are the van der Waals and electrostatic components of the pore/water interaction energy; $\Delta E^{VDW}_{PROTEIN/PROTEIN}$ and $\Delta E^{ELEC}_{PROTEIN/PROTEIN}$ are the van der Waals and electrostatic components of the protein/protein interaction energy for the pore subunits; and RMSD-Cα is the root mean square deviation of the Cα atoms of the pore model from the beginning to the end of the MD simulation.

The dynamics and orientation of the pore water molecules are summarized in Table 3. For these and subsequent models the water molecules are divided into three zones on the basis of their average z coordinate over the MD trajectory: "Cap-N" corresponds to those water molecules at the N-terminal mouth of the pore (for which $z < -15$ Å); "Pore" corresponds to those water molecules within the lumen of the pore (for which $|z| < 15$ Å); and "Cap-C" corresponds to those waters at the C-terminal mouth ($z > +15$ Å). We will discuss the waters of AN5 before drawing comparisons with AN6.

Waters within the lumen of the pore are preferentially oriented relative to the pore axis. In Fig. 1 *a*, it can be seen that the water molecules in the narrow column are oriented such that their oxygen atoms point downward, i.e., toward the N-terminal mouth of the pore. This may be quantified by calculating the value of μ_Z for each water molecule and averaging this value for the three zones defined above. For the pore zone the mean value of μ_Z is 62% of the maximum possible value if all waters were aligned such that their dipoles pointed exactly parallel to z, i.e., from the N-terminal to the C-terminal mouth of the pore. Thus there is a preferred orientation of water molecules within the pore. Examination of μ_Z for individual water molecules as a function of the z coordinate of their oxygen atoms (Fig. 2 *b*) shows that in the center of the pore the value of μ_Z rises to ~2 Debye, i.e., 85% of the maximum possible value. Such coupling of the helix dipole (i.e., peptide bond dipoles) with the water dipoles accounts for the favorable pore/water interaction energy of these hydrophobic pores.

Let us now consider the dynamic properties of the water molecules. For comparison (Table 3), D, τ_1^{-1}, and τ_2^{-1} for bulk water are listed, both experimental values (Eisenberg and Kauzmann, 1969) and values from a simulation of 231 modified TIP3 waters in the bulk state. Comparing waters in the cap and pore zones of AN5 with bulk water reveals that a) translational and rotational mobility within the lumen of the pore are reduced relative to the cap zones and b) mobility in the cap zones is comparable to that observed in the bulk water simulation. In Fig. 3 *a* a plot of the $\langle r(t)^2 \rangle$ vs. t curves averaged across all pore waters and all cap waters is shown. Comparable plots of averages of $C_1(t)$ and $C_2(t)$ are shown in Fig. 3, *b* and *c*, respectively. These confirm the difference in mobility between the cap and pore waters, and show that the analysis of mobilities described above (in Methods) is valid for both classes of water. If one examines D and τ_2^{-1} as functions of the average z coordinates of the waters (Fig. 2, *c* and *d*), it is evident that for those waters in the narrowest region of the pore (see Fig. 2 *a*), both D and τ_2^{-1} are reduced by a factor of 10 relative to their bulk water values. Thus significant immobilization of water occurs within the lumen of the AN5 pore. However, no significant difference between the D_{XY} and D_Z values for the pore water (Table 3) is observed, indicating that the reduction in translational mobility is in directions both parallel to and perpendicular to the pore axis.

It is important to test whether a 100-ps MD simulation is sufficiently long to characterize the structural and dynamic properties of pore waters. From examination of the trajectories of the dipole orientations of individual water molecules within the pore (Fig. 3 *d*) it is evident that the pore waters align themselves with their dipoles antiparallel to the helix dipoles in less than 20 ps. In contrast, the orientation of the cap water fluctuates markedly between their different orientations on the same time scale. To explore more systematically the effects of simulation duration on the analysis of water dynamic properties, simulation AN5 was repeated, but for a total duration of 500 ps (i.e., simulation AN5/500). Analysis of water dynamic parameters for AN5/500 (Table 3) reveals no significant difference from those derived from the corresponding 100-ps simulation (AN5).

To examine the sensitivity of the results to possible artefacts introduced by the use of atom-based cutoffs to truncate long-range electrostatic interactions, simulation AN5 was repeated using group-based cutoffs for electrostatic interactions, yielding simulation AN5/G. As can be

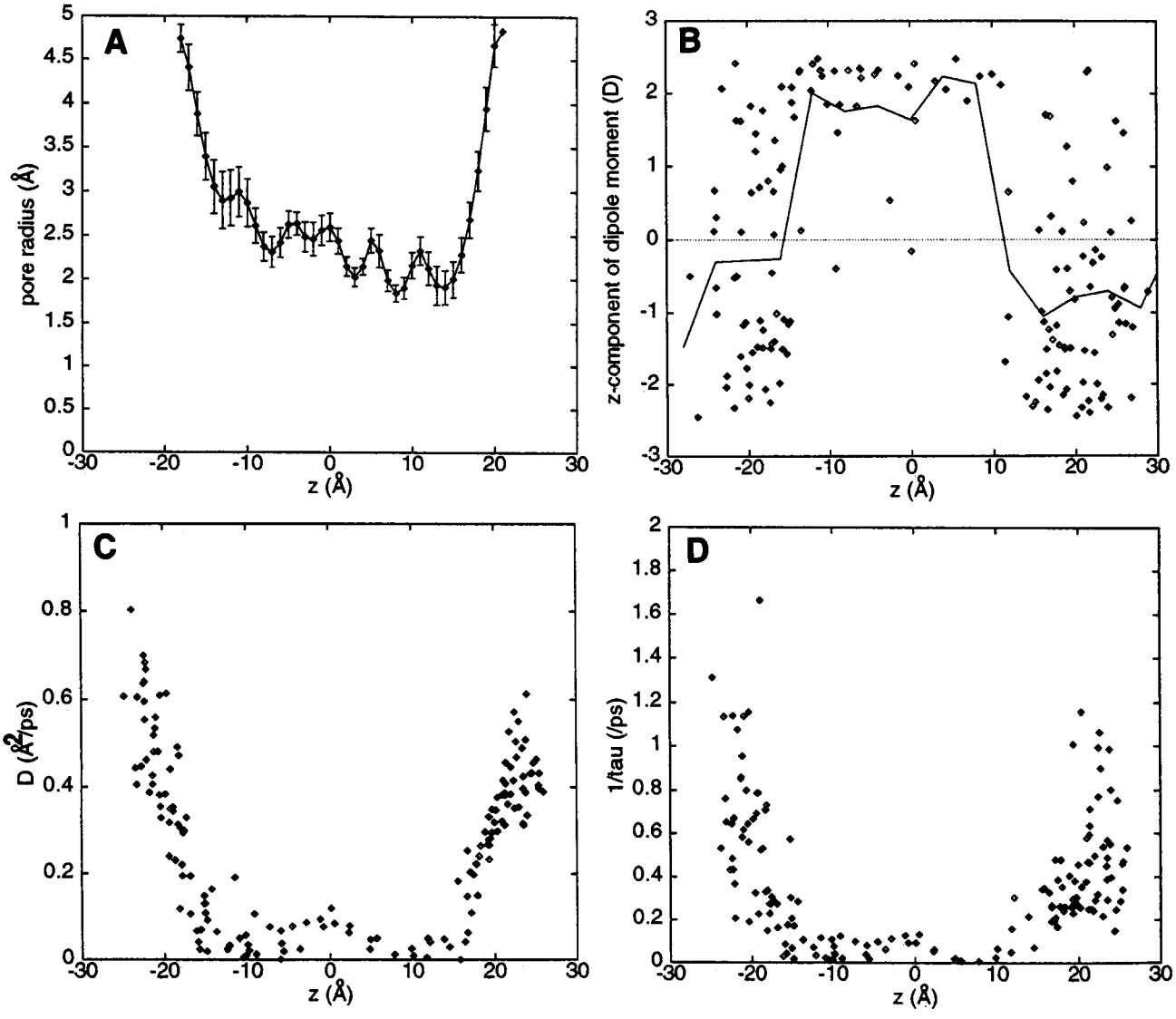

FIGURE 2 AN5 solvent structure and dynamics. (*a*) The pore radius profile. Each point represents the mean (error bars, ±SD) pore radius calculated across structures saved every 5 ps during the MD trajectory. (*b*) Water dipole orientation profile. The points represent μ_Z for each water molecule, calculated from the structure at the end of the MD simulation. The solid line represents the running average of the μ_Z values. (*c*) Self-diffusion coefficient profile. The self-diffusion coefficient (D) is plotted for each water molecule as a function of the average water oxygen z coordinate for the trajectory. (*d*) Dipole reorientation rate profile. The second-order water dipole reorientation rate (τ_2^{-1}) is plotted for each water molecule as a function of the average water oxygen z coordinate for the trajectory.

seen from Table 2, this does not alter the conclusions concerning the energetics of pore/water interactions. Similarly (Table 3), the use of group-based cutoffs did not significantly alter the dynamic or structural properties of the intra-pore water. Thus, in all subsequent simulations, atom-based cutoffs were retained.

Examination of water behavior in AN6 (Table 3) reveals the same overall pattern as for AN5. The dipole orientation effect is as strong as for AN5. However, the degree of immobilization is a little less than for AN5, reflecting the increased radius of the pore. The D and τ_2^{-1} profiles versus z (not shown) are the same shape as those for AN5.

Simulations BN8S8 and BN8S12

These simulations were performed in essentially the same manner as AN5 and AN6. As before, water molecules were added by taking a pre-equilibrated cylinder of waters (length, 60 Å; radius, 9.5 Å for BN8S8, 10.0 Å for BN8S12) and removing all water molecules closer than 1.6 Å to protein atoms plus those in the "pore" zone lying outside the helix bundle. Again, a cylindrical restraining potential was applied to the waters. For BN8S8 the radius of the restraint cylinder was 10.5 Å; for BN8S12 it was 11.0 Å. No other restraints were applied.

TABLE 3 Ala_N model pores: water properties

Model	Zone	N_W	D(Å^{2}ps^{-1})	D_{XY} (Å^{2}ps^{-1})	D_Z (Å^{2}ps^{-1})	τ_1^{-1} (ps^{-1})	τ_2^{-1} (ps^{-1})	μ_Z (D)
Bulk water (experimental)	—	—	0.23 [1]	—	—	0.21 [1]	0.52 [2]	—
Bulk water (modified TIP3P)	All	231	0.32 (10.12)	—	—	0.30 (0.16)	0.64 (0.28)	−0.02 (1.45)
AN5	Cap-N	55	0.31 (0.16)	0.30 (0.17)	0.35 (0.22)	0.19 (0.10)	0.56 (0.35)	−0.43 (1.39)
	Pore	40	0.05 (0.05)	0.04 (0.04)	0.06 (0.06)	0.03 (0.03)	0.08 (0.07)	+1.45 (1.35)
	Cap-C	65	0.31 (0.11)	0.33 (0.14)	0.26 (0.16)	0.22 (0.11)	0.44 (0.24)	−0.83 (1.23)
AN5/500	Cap-N	48	0.36 (0.14)	0.36 (0.15)	0.35 (0.16)	0.15 (0.06)	0.27 (0.13)	+0.01 (1.45)
	Pore	52	0.08 (0.05)	0.07 (0.06)	0.09 (0.07)	0.04 (0.03)	0.09 (0.04)	+1.61 (0.97)
	Cap-C	60	0.29 (0.11)	0.30 (0.14)	0.25 (0.11)	0.17 (0.05)	0.31 (0.12)	−0.39 (1.26)
AN5/G	Cap-N	41	0.38 (0.18)	0.40 (0.20)	0.32 (0.18)	0.21 (0.13)	0.54 (0.36)	+0.03 (1.38)
	Pore	69	0.08 (0.05)	0.07 (0.05)	0.09 (0.08)	0.02 (0.03)	0.06 (0.05)	+1.95 (0.78)
	Cap-C	50	0.26 (0.13)	0.27 (0.13)	0.22 (0.17)	0.24 (0.16)	0.44 (0.27)	−0.23 (1.66)
AN6	Cap-N	70	0.28 (0.15)	0.29 (0.17)	0.25 (0.16)	0.21 (0.12)	0.50 (0.27)	−0.27 (1.41)
	Pore	99	0.08 (0.05)	0.07 (0.05)	0.09 (0.07)	0.04 (0.03)	0.11 (0.07)	+1.54 (1.01)
	Cap-C	72	0.27 (0.13)	0.29 (0.16)	0.23 (0.15)	0.19 (0.11)	0.42 (0.22)	−0.39 (1.43)
BN8S8	Cap-1	83	0.29 (0.14)	0.32 (0.19)	0.23 (0.11)	0.21 (0.10)	0.45 (0.22)	+0.15 (1.44)
	Pore	114	0.09 (0.08)	0.09 (0.08)	0.10 (0.10)	0.10 (0.08)	0.22 (0.18)	+0.03 (1.51)
	Cap-2	96	0.38 (0.17)	0.39 (0.19)	0.35 (0.20)	0.23 (0.11)	0.56 (0.24)	−0.12 (1.52)
BN8S12	Cap-1	107	0.37 (0.15)	0.39 (0.19)	0.33 (0.19)	0.28 (0.12)	0.57 (0.20)	+0.06 (1.43)
	Pore	160	0.15 (0.10)	0.15 (0.11)	0.15 (0.12)	0.17 (0.10)	0.32 (0.20)	+0.10 (1.49)
	Cap-2	116	0.40 (0.14)	0.41 (0.18)	0.39 (0.21)	0.28 (0.13)	0.59 (0.25)	−0.22 (1.38)

Zones: Cap-N and Cap-C, N- and C-terminal caps for α-helix bundles; Cap-1 and Cap-2, caps for β-barrels; Pore, pore. N_W is the number of water molecules in a zone; D is their self-diffusion coefficient; τ_1^{-1} and τ_2^{-1} are the first- and second-order rotational reorientation rates; and μ_z is the projection of the water molecule dipole onto the pore (i.e., z) axis. All values are given as mean (SD) for all water molecules in a zone. Two sets of parameters are given for "bulk" water: experimental values ([1], Eisenberg and Kauzmann, 1969; [2], Rahman and Stillinger, 1971); and values for a simulation of 231 modified TIP3P waters in a $(19.042)^3$ Å^3 box of water, using periodic boundaries.

The structure of BN8S8 at the end of the MD simulation is shown in Fig. 1 *b*. It is evident that the pore is wider than that of AN5, and there does not appear to be any preferential orientation of the water dipoles within the lumen of the pore. The pore radius profile for BN8S8 (Fig. 4 *a*) reveals a pore of radius 3 to 3.5 Å, i.e., comparable to that of AN6, whereas the mean radius of BN8S12 is ~4.5 Å. Comparison of the models before and after solvation and 100-ps MD revealed no significant changes in the geometry of the barrels. Some fraying of H-bonding between the β-strands occurred at their extremities, resulting, in BN8S8, in somewhat more extensive disruption of H-bonding between two of the strands. This is the cause of the higher Cα RMSD for BN8S8 (Table 2) but does not result in any major distortion of the pore.

The energetics of β-barrel pore models are different from α-helix bundles. There is a large favorable electrostatic term for the protein/protein interactions, reflecting interstrand H-bonding. The strength of the electrostatic interaction between the pore and the water is significantly reduced relative to AN5 and AN6, reflecting a difference in the nature of the pore/water interactions. This difference is evident once one examines the water dipole orientations for β-barrel models (Table 3). No significant alignment of water dipoles relative to the pore axis is found. This is confirmed if one examines μ_Z versus z (Fig. 4 *b*), which reveals a random distribution of water dipoles relative to the pore axis. Evidently the absence of a net pore dipole for β-barrel models weakens pore/water electrostatic interactions, and so preferential orientation of water molecules does not take place.

Despite the absence of dipole orientation of the intra-pore waters in BN8S8 and BN8S12, the waters in the lumen of the pore are immobilized relative to bulk water. Table 3 reveals a small but consistent reduction of translational and rotational mobility within the β-barrel pores. This is more evident when one examines the profiles along z of D and of τ_2^{-1} for BN8S8 (Fig. 4, *c* and *d*). Comparison of BN8S12 with BN8S8 reveals that the reduction of mobility is greater for the narrower pore. However, if one compares BN8S8 with AN6, bearing in mind that the pores are of about the same radius, it is evident that the degree of rotational immobilization is greater for AN6. This correlates with the helix/water dipole coupling in AN6. Thus, our studies on water molecules within hydrophobic pores suggest that confinement within a polypeptide pore reduces both translational and rotational mobility, and that electrostatic effects may enhance the latter effect.

Simulation δ-ToxN6

This simulation model provides an opportunity to examine the behavior of water within a hydrophilic pore. Water molecules were added to the model of the pore using the same protocol as for AN5 and AN6. The presence of polar side chains reduced problems with evaporation of waters during the MD simulation, so a restraining potential was only placed on the water molecules at the mouths of the pore, in the form of a planar potential at $z = -30$ Å and $z = +30$ Å. Thus, within the region -30 Å $< z < +30$ Å the

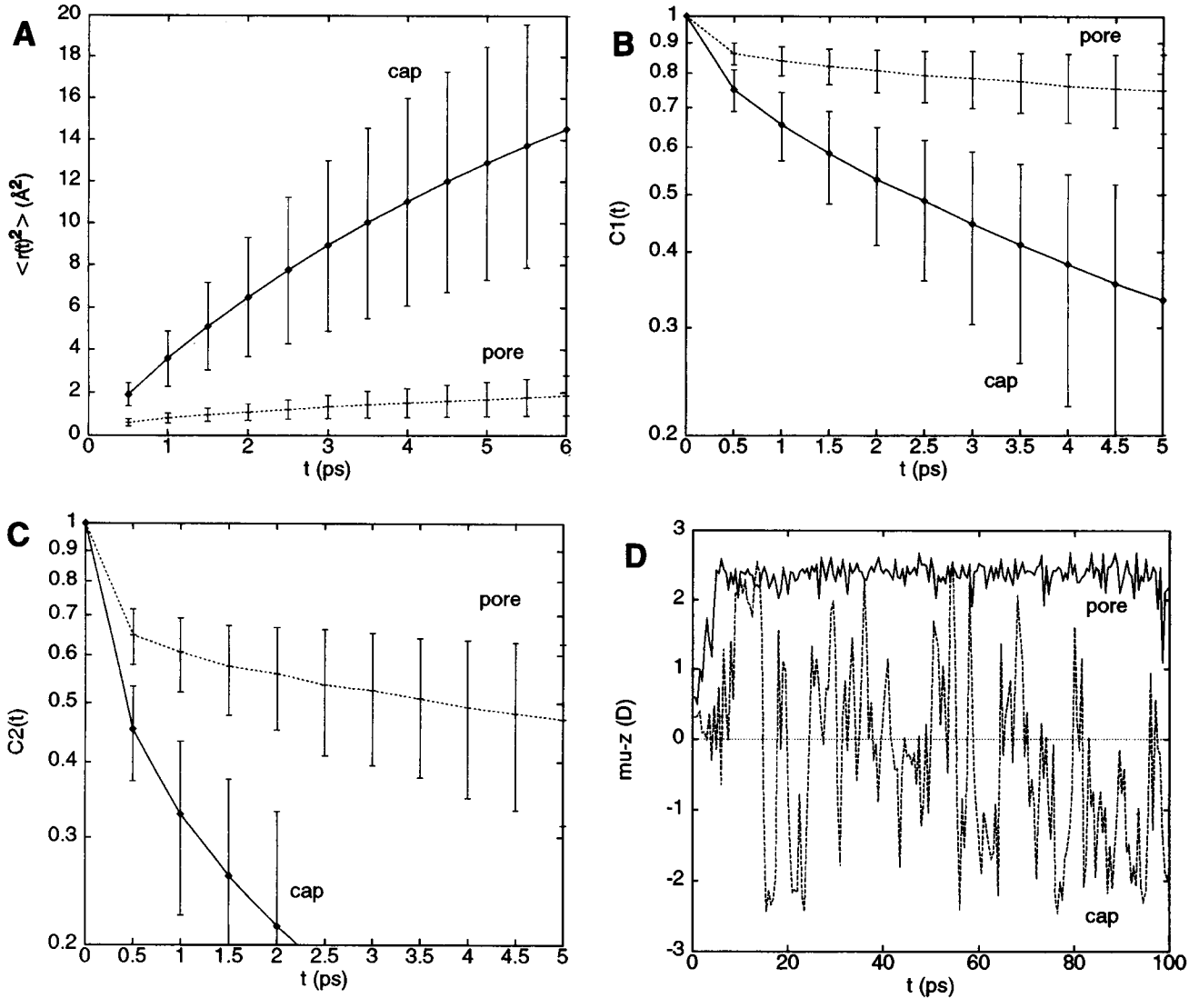

FIGURE 3 Analysis of dynamics for simulation AN5. (*a*) Plots of mean square deviation, i.e., $\langle r(t)^2 \rangle$ vs. t (see Eq. 4), for the cap and the pore waters. The two curves represent averages for a give zone (with ±SD as error bars). (*b*) Rotational correlation function $C_1(t)$ for cap and pore waters. (*c*) Rotational correlation function $C_2(t)$ for cap and pore waters. (*d*) Trajectories of the z axis projection of the dipole moment for two individual water molecules, one from the pore zone and one from the cap.

waters were unrestrained. Intra-helical distance restraints (from O_i to H_{i+4}) were employed, as in the initial generation of the δ-ToxN6 pore model by SA/MD (Kerr et al., 1996), to maintain the δ-toxin monomers in an α-helical conformation.

The structure of the δ-ToxN6 pore is illustrated in Fig. 5 *a*. As in AN5 and AN6 the helices form a left-handed coiled coil, and the structure of the helix bundle did not change greatly after solvation and 100-ps MD simulation. Thus, in the initial model $R = 9.6\ (\pm 0.5)$ Å and $\Omega = +18.9\ (\pm 2.3)°$, whereas after solvation and 100-ps MD $R = 10.3\ (\pm 0.1)$ Å and $\Omega = +16.1\ (\pm 8.2)°$. The Cα RMSD for δ-ToxN6 is the same as that for AN6.

The mean pore radius for the N-terminal two-thirds of the δ-ToxN6 pore is about the same as that for AN6, i.e., 4 Å. Close to the C-terminus the pore is constricted to a radius of ~2.5 Å (Fig. 6 *a*) by a ring of Lys-25 side chains. The fluctuations in the C-terminal pore radius (evident from the error bars of Fig. 6 *a*) are due to changes in conformation of these side chains.

The energetics of δ-ToxN6 (Table 2) reveal the interactions of the polar, pore-lining side chains. The electrostatic components of protein/protein and of pore/water interaction energies are large and favorable. The favorable protein/protein interaction energy reflects the formation of interhelix H-bonds (Kerr et al., 1996). The highly favorable pore/water interaction energy reflects the formation of numerous H-bonds between intra-pore waters and side chains of the pore-lining residues.

Strong interactions of pore waters with polar and charged side chains result in an inversion of the water dipole orientation relative to that seen in AN5 and AN6. From Fig. 5 *a*

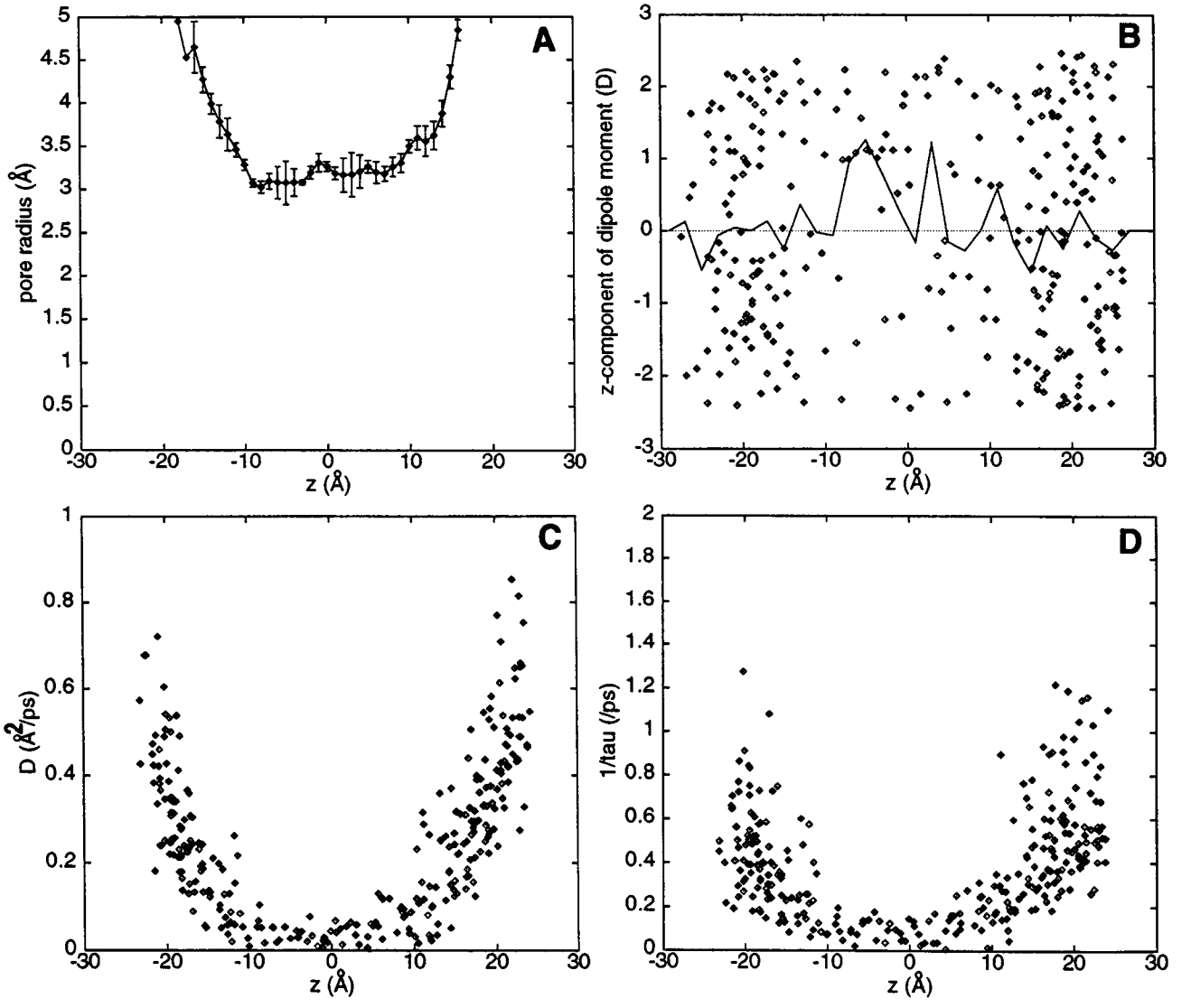

FIGURE 4 BN8S8 solvent structure and dynamics. (*a*) The pore radius profile. (*b*) Water dipole orientation profile. (*c*) Self-diffusion coefficient profile. (*d*) Dipole reorientation rate profile.

it can be seen that most of the intra-pore waters have their oxygen atoms pointing toward the C-termini of the helices. This inversion is even more obvious from the plot of μ_Z versus z (Fig. 6 *b*). Within the center of the pore, μ_Z falls to ~ -1.5 Debye, i.e., -64% of the value expected if the water dipoles were aligned exactly parallel to z. Inversion of the water orientation reflects the pattern of charged side chains along the δ-toxin sequence (Table 1). Thus, the N-terminal half of the helix contains two anionic side chains (Asp-4 and Asp-11), whereas there are three positively charged side chains (Lys-22, Lys-25, and Lys-26) at the C-terminus. Simple electrostatics calculations (Kerr et al., 1996) indicate that this distribution of side chains is sufficient to reverse the effect of the helix dipoles on the net electrostatic field experienced along the pore axis. In addition to the inversion of the orientation of the pore waters relative to AN5, the mean orientation of the waters at the pore mouths is also inverted.

The changes in dynamics of waters along the pore axis are slightly obscured by the relatively small numbers of waters included at the pore mouths in this model (Table 4). However, it is evident that the translational and rotational mobility of waters within the pore lumen is significantly lower than that of bulk water and is lower than that of the cap waters. In general the pore water is slightly more mobile than, e.g., in the AN6 pore. The variation of D and τ_2^{-1} along the pore axis (Fig. 6, *c* and *d*) reveals an interesting correlation with the pore radius profile (Fig. 6 *a*). Thus, the lowest mobility correlates with the constriction of the channel close to its C-terminal mouth, at $z = +10$ Å.

The clear partitioning of side chains in δ-ToxN6, between the hydrophilic side chains lining the pore and the hydro-

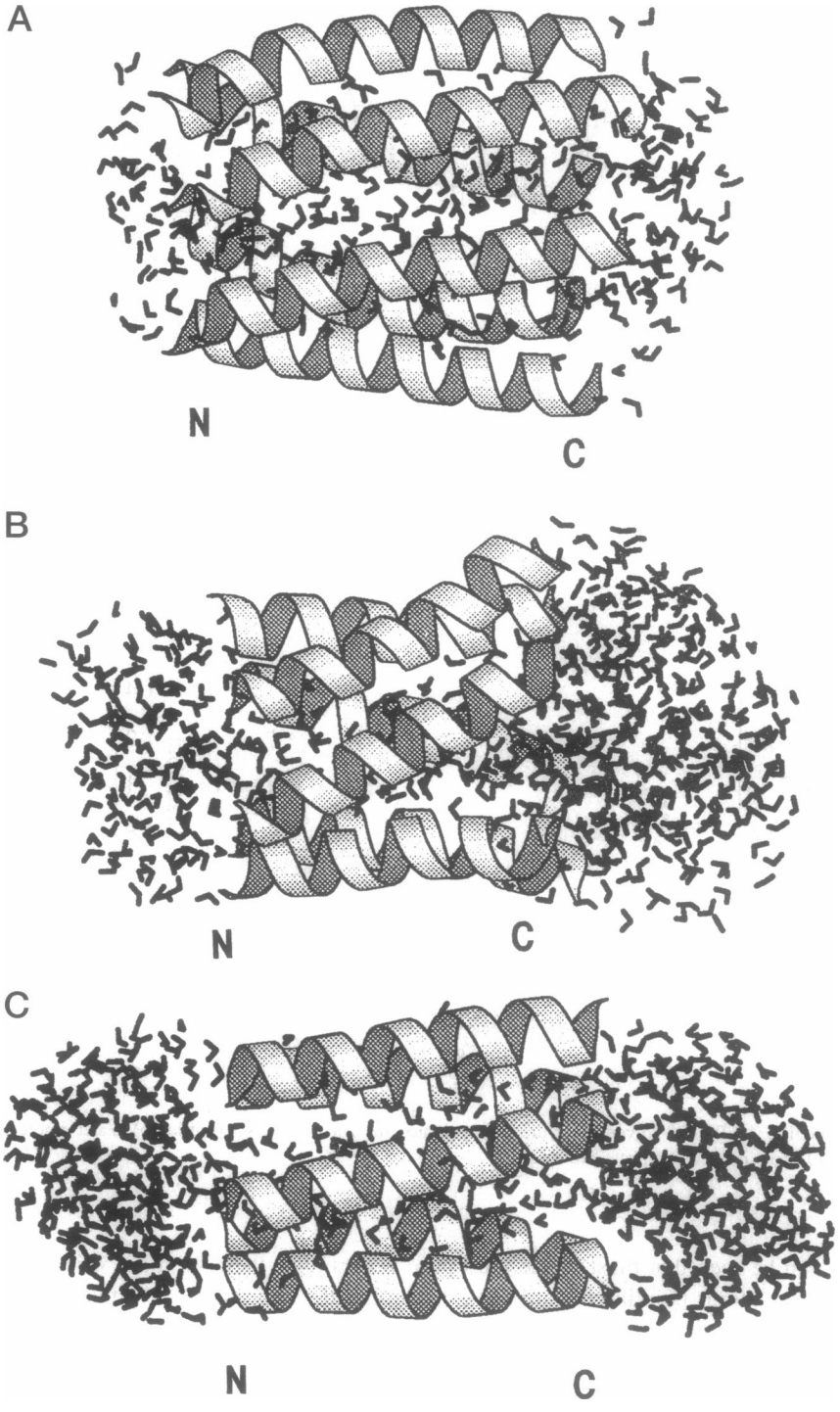

FIGURE 5 Pores formed by amphipathic helix bundles. Molscript-generated diagrams of the structures of models (*a*) δ-ToxN6, (*b*) AlmN6, and (*c*) at the end the MD simulation.

phobic side chains covering the outside of the helix bundle, enabled us to determine whether there was any pronounced difference in side-chain mobility between the inside and outside of the pore. Side-chain mobility was measured at the total number of χ_1 transitions (i.e., between $g+$, $g-$, and t) for a given residue during the course of the simulation. Display of the frequency of such transitions as a function of residue position within the sequence (Fig. 7 *a*) reveals that there is no simple correlation between hydrophilicity/hydrophobicity and residue mobility. The results do show significant mobility for the two lysines (Lys-25 and Lys-26) that guard the C-terminal mouth of the pore. It was of interest to examine whether the motions of these side chains correlated with that of waters into and out of the C-terminal mouth of the pore. To this end we traced the movements of water molecules which at some stage in the trajectory formed H-bonds to Lys-26 of one of the helices. These showed variable patterns of correlation between Lys and water

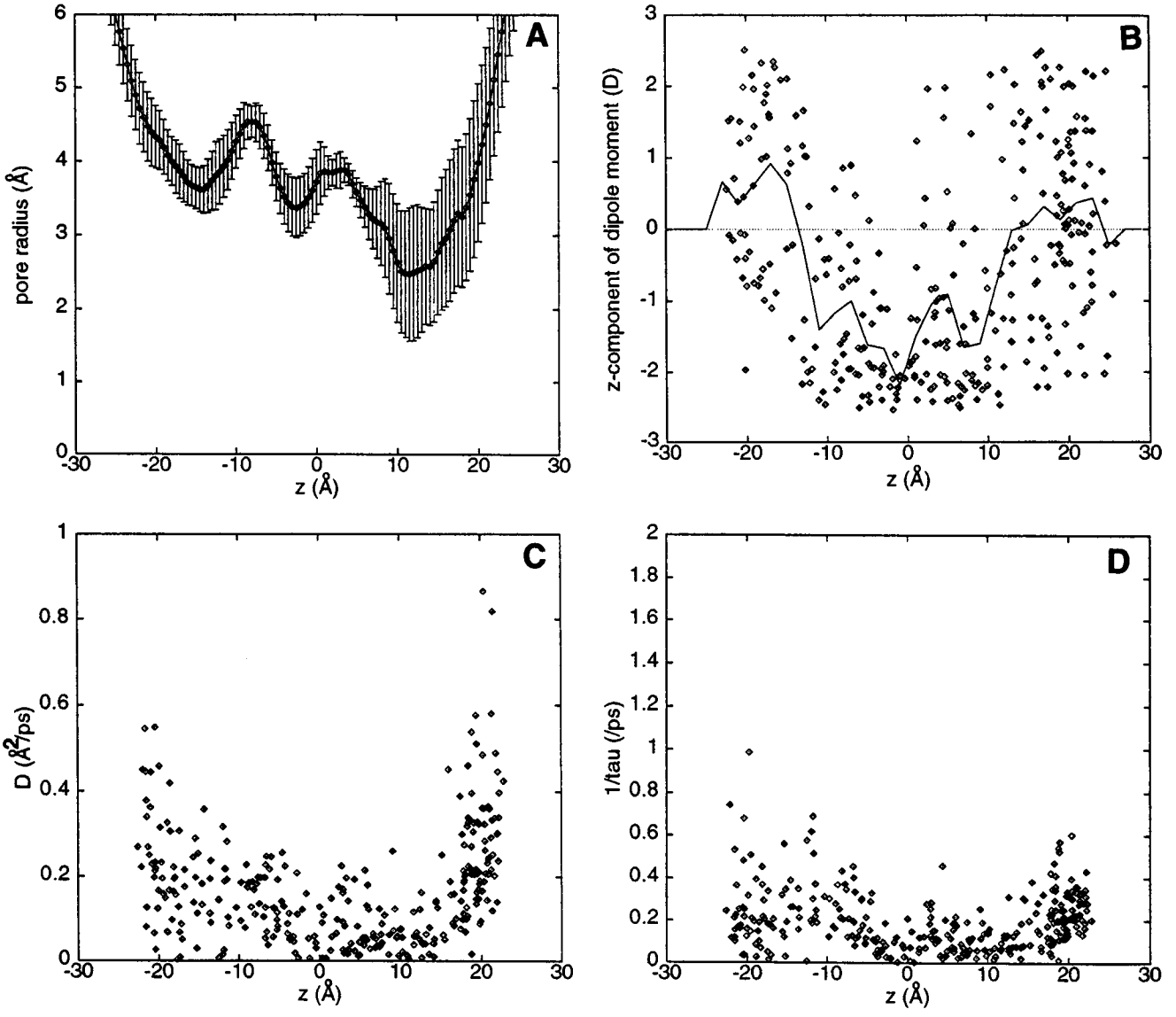

FIGURE 6 δ-ToxN6 solvent structure and dynamics. (*a*) The pore radius profile. (*b*) Water dipole orientation profile. (*c*) Self-diffusion coefficient profile. (*d*) Dipole reorientation rate profile.

movements. In Fig. 7, *b*, *c*, and *d*, three examples of differing degrees of correlation are shown. Water-297 (Fig. 7 *b*) forms an H-bond to Lys-26 (of helix 1) for over 90 ps. During this time the movement (on *z*) of the water and the lysine amino group are highly correlated. Water-232 (Fig. 7 *c*) shows intermediate behavior—for the first 50 ps it is in the Cap-C zone. It then forms an H-bond to Lys-26 as it moves into the pore, and subsequently the motions of water and the side chain are highly correlated. Water-70 (Fig. 7 *d*) shows the opposite extreme of behavior. It sits close to the mouth of the pore and only forms a transient H-bond to Lys-78 (i.e., Lys-26 of helix 3). Its movements on *z* are not correlated with those of the side chain. From inspection of these and other comparable trajectories it would appear that there is no simple rule governing the coupling of side-chain and water motions at the mouths of the pore, although it is clear that in some cases the waters do move in a concerted fashion with the flexible side chains.

Simulations AlmN6 and AlmN8

These two models present the opportunity to explore water dynamics in a model pore of more complex geometry and for which different sizes of pores (in terms of numbers of helices per bundle) exist. The initial models were generated by SA/MD (Sansom, 1993; Breed and Sansom, 1994) such that the N-terminal helical segments were closely packed together. To maintain this close packing inter-helix distance restraints were employed between the N-terminal helix seg-

TABLE 4 δ-Toxin, Alm, and M2α7 pores: water properties

Model	Zone	N_W	D(Å^{2}ps^{-1})	D_{XY} (Å^{2}ps^{-1})	D_Z (Å^{2}ps^{-1})	τ_1^{-1} (ps^{-1})	τ_2^{-1} (ps^{-1})	μ_Z (D)
δ-ToxN6	Cap-N	23	0.25 (0.15)	0.30 (0.20)	0.16 (0.18)	0.11 (0.06)	0.25 (0.18)	+0.41 (1.1)
	Pore	219	0.12 (0.09)	0.12 (0.10)	0.13 (0.11)	0.07 (0.06)	0.17 (0.13)	−0.73 (1.5)
	Cap-C	75	0.27 (0.16)	0.32 (0.20)	0.17 (0.14)	0.13 (0.07)	0.26 (0.11)	+0.24 (1.1)
AlmN6	Cap-N	139	0.38 (0.25)	0.43 (0.34)	0.27 (0.29)	0.25 (0.14)	0.54 (0.29)	−0.20 (1.31)
	Pore	181	0.14 (0.11)	0.14 (0.13)	0.13 (0.16)	0.12 (0.11)	0.26 (0.19)	+0.37 (1.53)
	Cap-C	272	0.39 (0.20)	0.43 (0.26)	0.32 (0.28)	0.26 (0.14)	0.58 (0.29)	−0.67 (1.33)
AlmN8	Cap-N	207	0.43 (0.23)	0.50 (0.31)	0.31 (0.25)	0.27 (0.16)	0.58 (0.28)	+0.03 (0.60)
	Pore	335	0.17 (0.12)	0.17 (0.13)	0.16 (0.17)	0.18 (0.10)	0.31 (0.26)	+0.87 (1.06)
	Cap-C	241	0.45 (0.23)	0.51 (0.30)	0.34 (0.26)	0.26 (0.16)	0.59 (0.28)	−0.55 (0.45)
M2α7N5	Cap-N	229	0.27 (0.13)	0.29 (0.15)	0.23 (0.13)	0.25 (0.17)	0.61 (0.45)	−0.07 (1.51)
	Pore	185	0.08 (0.05)	0.08 (0.05)	0.09 (0.07)	0.08 (0.06)	0.16 (0.11)	+0.98 (1.32)
	Cap-C	277	0.27 (0.10)	0.28 (0.12)	0.24 (0.13)	0.31 (0.17)	0.68 (0.43)	−0.44 (1.39)

Zones: Cap-N and Cap-C, N- and C-terminal caps for α-helix bundles; Cap-1 and Cap-2, caps for β-barrels; Pore, pore. N_W is the number of water molecules in a zone; D is the self-diffusion coefficient; D_{XY} and D_z are the self-diffusion coefficients in the xy plane (i.e., perpendicular to the pore axis) and along z (i.e., parallel to the pore axis); τ_1^{-1} and τ_2^{-1} are the first- and second-order rotational reorientation rates; and μ_z is the projection of the water molecule dipole onto the pore (i.e., z) axis. All values are given as mean (SD) for all water molecules in a zone.

ments. Because of the looser packing of the C-terminal segments (which were not subject to inter-helix distance restraints) it was necessary to employ a cylindrical restraining potential on the water molecules. The water molecules were added to the pore models by a two-stage solvation procedure. In the first stage a 10-Å sphere of pre-equilibrated waters was centered on each amino acid residue in turn, and waters not overlapping with either protein or other water atoms were retained. Water molecules outside the bundle pore or the cap regions were then discarded. The second stage of solvation repeated the first stage, this time placing the 10-Å sphere on all of the first-stage waters as well as the amino acids. The second stage of solvation had the effect of increasing the size of the two caps of water at either mouth of the pore.

The structure of the AlmN6 pore is illustrated in Fig. 5 *b*. Two features are evident: a) the caps of water molecules are larger than for δ-ToxN6, thus allowing improved statistical analysis of differences in water parameters between the cap and pore zones; b) the C-terminal helical segments splay outward. The latter is a result of the flexibility of the Alm helices at their central Pro-14-induced kinks, combined with the electrostatic repulsions between their Glu-18 residues. Consequently the pore is much wider at its C-terminal mouth than at its N-terminal mouth: for AlmN6 the radius is ~2 Å at the N-terminus and ~5 Å at the C-terminus; for AlmN8 the radius increases from ~5 Å to ~7 Å. The Cα RMSDs for the two Alm simulations are somewhat higher than for the other helix bundles, also reflecting the flexibility of the C-terminal helical segments in Alm pores.

The energetics of protein/protein interactions for AlmN6 and AlmN8 are similar to those for AN5 and AN6. The electrostatic interaction is weakly unfavorable, reflecting the balance of favorable inter-helix H-bonds in the vicinity of Gln-7 and of electrostatic repulsion in the vicinity of the Glu-18 ring at the C-terminal mouth. Pore/water interactions are favorable and are dominated by the electrostatic term, because of the favorable interactions of water molecules with polar side chains (Gln-7, Glu-18, and Gln-19) and with the exposed main-chain carbonyl oxygens in the vicinity of the proline-induced kink.

Focusing on AlmN6, the values of μ_Z for the three zones of the pore (Table 4) suggest that alignment of water dipoles parallel to the pore (z) axis occurs, but that this is not pronounced. However, inspection of μ_Z versus z (Fig. 8 *b*) reveals a more complex pattern. For the N-terminal half of the pore (-15 Å $< z < 0$ Å), in which the helices are closely packed, waters are oriented such that μ_Z assumes ~75% of its maximum value. A weakening of water dipole alignment occurs in the C-terminal half of the pore, which is wider and contains the ring of anionic residues. Thus maximum preferential orientation of the water dipoles occurs in the narrowest region of the pore.

Water dynamic properties show a similarly complex pattern. Comparing the cap and pore zones reveals a degree of immobilization of waters within the pore. Fig. 8, *c* and *d*, reveals a clear correlation between the loss of mobility of water molecules and the radius of the pore. Thus, in the narrowest region of the pore ($z = -10$ Å, pore radius ~1.8 Å) both translational and rotational mobilities are reduced by approximately an order of magnitude relative to the bulk simulation. There is then a gradual increase in the average mobility as the pore widens from its N- to its C-termini.

If one compares AlmN8 with AlmN6 the patterns of water dipole orientation and water dynamics are the same. The greater overall pore radius of AlmN8 relative to AlmN6 does not appear to reduce the degree of orientation of the water dipoles, but it does reduce the effect on water mobility. This is in agreement with the results from comparing AN5 and AN6.

Simulation M2α7N5

M2α7N5 is an approximate model of the pore of the nAChR. As such it does not take into account the kinking of the M2 helices observed in the intact protein (Sansom et al., 1995; Unwin, 1995) and so is more representative of pores

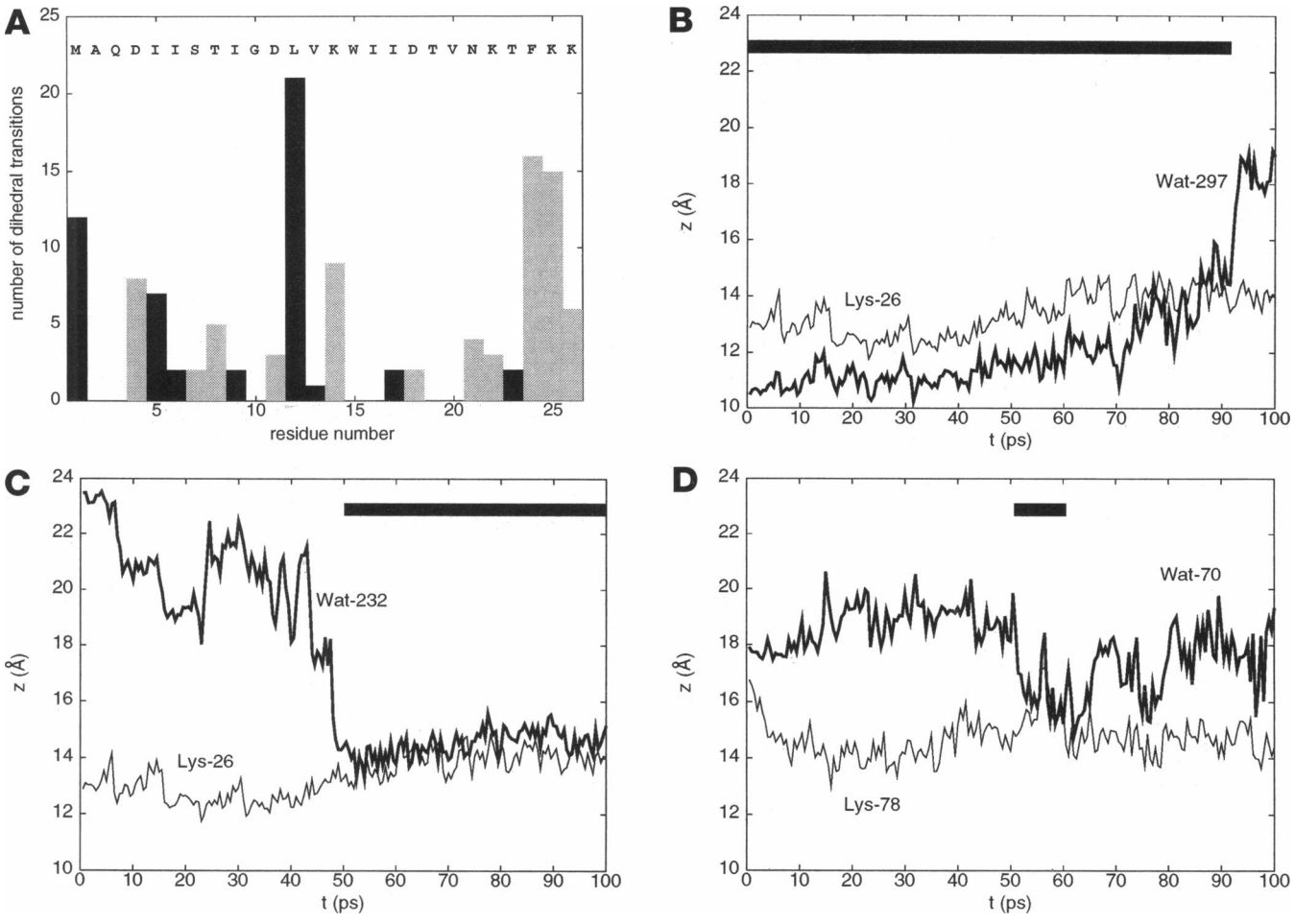

FIGURE 7 δ-ToxN6 side-chain dynamics. (*a*) The number of side-chain dihedral (γ_1) transitions, summed over all six helices, is shown as as a function of residue number. Black bars correspond to hydrophobic side chains, grey bars to hydrophilic side chains. (*b–d*) Trajectories of the *z* coordinates of three selected water molecules in the Cap-C zone and of the corresponding lysine side chains to which they are H-bonded. In each case the bold line indicates the *z* trajectory of the water oxygen and the thin line that of the Nζ-atom of the lysine. The solid bar indicates the duration of the water/lysine H-bond.

formed by synthetic M2 peptides (Montal, 1995; Sankararamakrishnan and Sansom, 1995a,b). The helices are packed in a tilted fashion such that the C-terminal mouth of the pore is somewhat wider than the N-terminal mouth (Sankararamakrishnan and Sansom, 1995a,b). This is necessary to overcome electrostatic repulsion of Glu-22 residues of adjacent helices. It also enables large organic cations, e.g., the local anesthetic derivative QX222, which blocks both nAChR and M2 peptide channels to enter the pore at its C-terminal mouth and gain access to their binding site, which is close to the middle of the M2 sequence (Charnet et al., 1990). Both during the initial SA/MD run (Sankararamakrishnan and Sansom, 1995a) and during the MD simulation on the solvated bundle, tilting of the helices was maintained by inter-helix distance restraints. As in δ-ToxN6, intra-helix restraints were used to maintain an α-helical conformation. Restraints were not necessary to prevent evaporation of the water molecules from the pore, because of the rings of charged residues at either mouth of the pore, which interacted strongly with the waters. The pore model was solvated using an I-shaped box of 1000 TIP3P water molecules. This box was placed such that the top and bottom of the "I" corresponded to the caps at either mouth of the pore. Those water molecules that formed close contacts with protein atoms were then removed. Simulation M2α7N5 used XPLOR, rather than CHARMM, and a somewhat different MD protocol from that of the other simulations.

The structure of M2α7N5 is shown in Fig. 5 *c*. The caps of water molecules are quite extensive, and the pore is wider at the C-termini of the helices. Partly as a result of the inter-helix distance restraints, the packing of the helices did not alter significantly during the MD simulation, as revealed by the low value of the Cα RMSD. For the initial model the mean helix crossing angle was $\Omega = +9°$; after solvation and MD simulation this increased to $\Omega = +11°$. Thus the M2α7N5 bundle also corresponds to a left-handed coiled coil. The pore radius profile confirms that the pore widens as one moves from the N- to the C-terminal mouth, from a radius of ~2.5 Å to ~3.5 Å. There are constrictions along

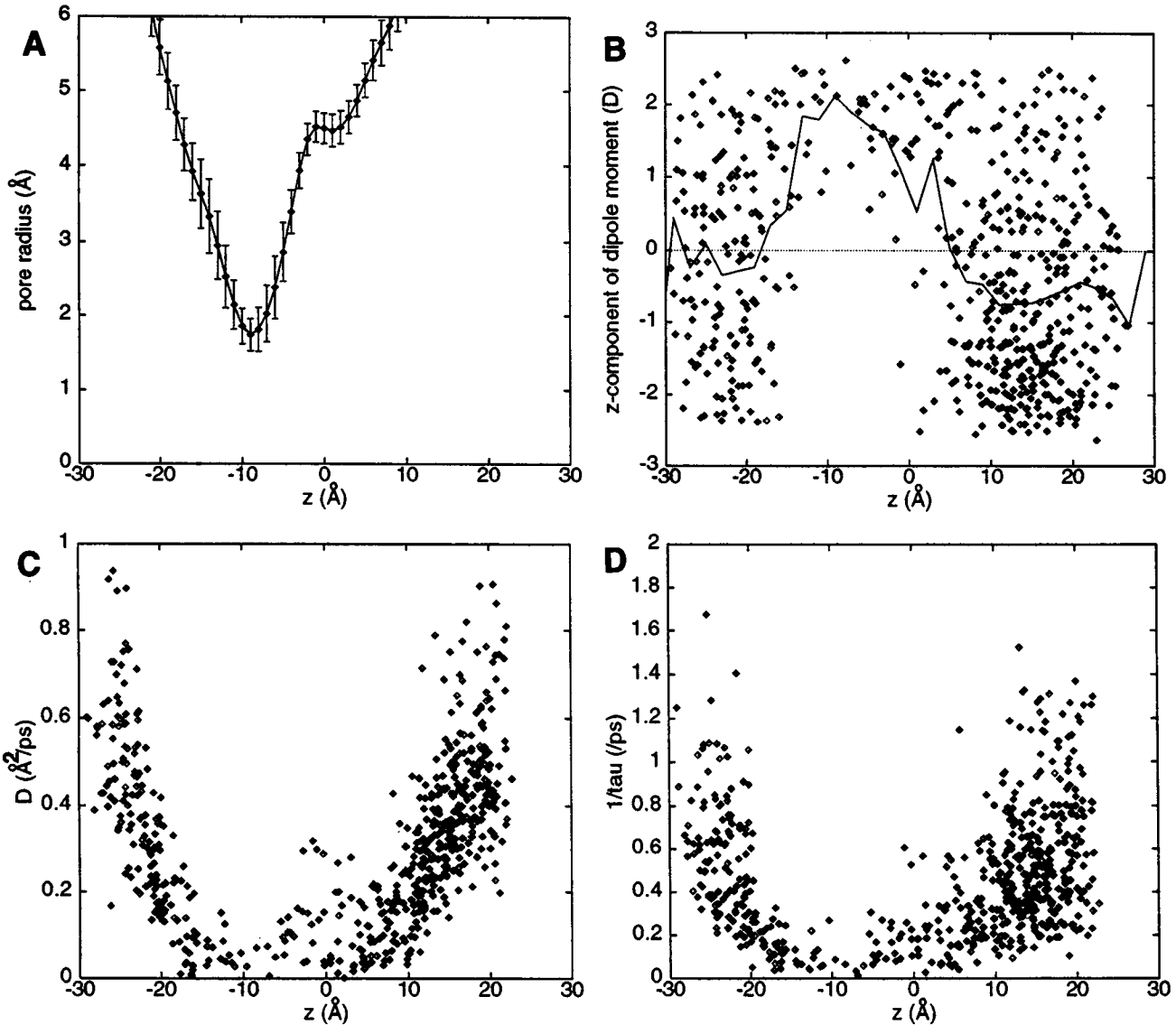

FIGURE 8 AlmN6 solvent structure and dynamics. (*a*) The pore radius profile. (*b*) Water dipole orientation profile. (*c*) Self-diffusion coefficient profile. (*d*) Dipole reorientation rate profile.

the pore corresponding to the rings of pore-lining side chains found in the nAChR (Bertrand et al., 1993).

The energetics of M2α7N5 (Table 2) reveal that helix-helix interactions are weak but favorable. As with other pores formed from amphipathic helices, there is a strong favorable electrostatic interaction between the pore and water molecules. This is mainly a result of the rings of anionic residues (Glu-1 and Glu-22) at either mouth of the pore and the rings of hydroxyl-containing residues (Ser-4, Thr-8, Ser-12) lining the N-terminal half of the pore.

Examination of Fig. 5 *c* shows that water molecules within the pore lumen are oriented such that their oxygens point toward the N-termini of the helices. This orientation of the water dipoles is confirmed by the statistical analysis (Table 4) and by the plot of μ_Z as a function of z (Fig. 9 *b*). Within the pore the mean value of μ_Z is $\sim$1.3 Debye, i.e., 55% of the maximum possible value. Inspection of the M2α7 sequence (Table 1) indicates that the distribution of side chains reinforces the helix dipole effect (as in Alm) rather than reversing it (as in δ-toxin).

The pattern of translational and rotational mobilities of waters within the M2α7N5 pore is similar to that for the Alm pores. Thus, at the narrowest region of the pore (z = -15 Å), D and τ_2^{-1} are reduced $\sim$5-fold relative to that of bulk water. There is a gradual increase in translational mobility along the length of the pore as the pore radius increases. Furthermore, a local widening of the pore midway down (at $z \sim 0$ Å; Fig. 9 *a*) seems to result in a small increase in D and τ_2^{-1} for those waters located in this region (Fig. 9, *c* and *d*). Thus, M2α7N5 confirms that the dynamic properties of the intra-pore waters are sensitive to the local geometry of the pore, in particular its radius. The overall similarity of the patterns of pore versus cap water dynamics, and of water dipole orientation for M2α7N5 and for the

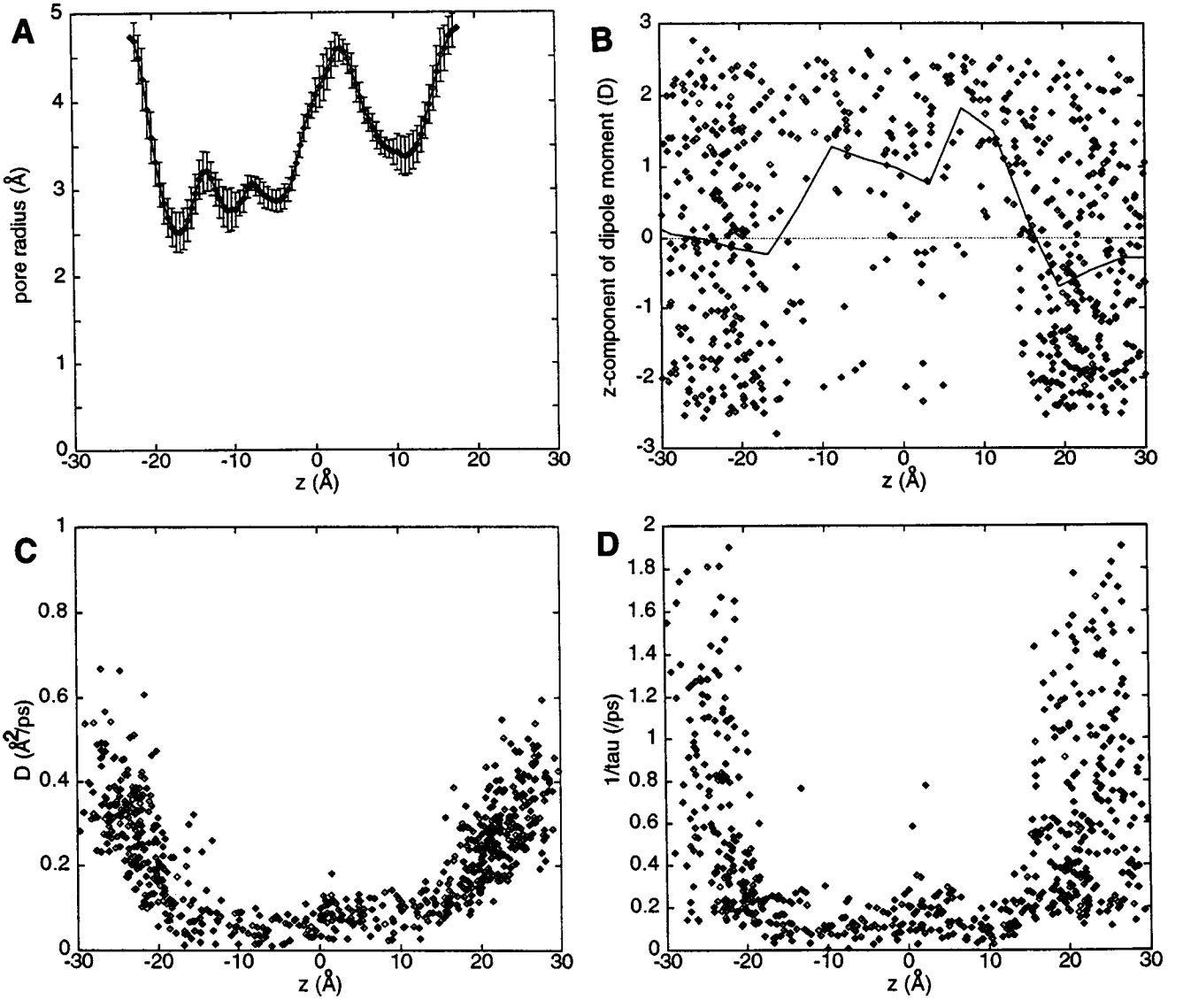

FIGURE 9 M2α7N5 solvent structure and dynamics. (*a*) The pore radius profile. (*b*) Water dipole orientation profile. (*c*) Self-diffusion coefficient profile. (*d*) Dipole reorientation rate profile.

other simulations, suggests that these results are relatively robust to small changes in simulation protocol.

DISCUSSION

Critique of methods

In any simulation study it is important to consider the extent to which the results are influenced by the conditions of the simulation. In the current study this requires examination of three aspects: a) the pore models employed; b) the water model employed; and c) the effects of restraints.

The pore models employed were all developed by SA/MD. This has been demonstrated to generate plausible models of pores formed by either parallel α-helix bundles (Kerr et al., 1994) or antiparallel β-barrels (Sansom and Kerr, 1995). In the absence of high-resolution structures for any trans-bilayer pores other than porins (Cowan et al., 1992), one cannot be certain that such models are correct. However, the models presented for the amphipathic helix bundles are supported by a substantial body of spectroscopic and/or crystallographic evidence for their secondary structure, plus indirect evidence for the overall architecture of the bundles (Sansom, 1991, 1993). The other limitation of the models is the absence of a lipid bilayer. Inclusion of an all-atom model for a bilayer would have rendered the computations prohibitively long. However, as the direct interactions of the water molecules are with one another and with the protein atoms lining the pore, the omission of a lipid bilayer may be an acceptable first approximation.

The second aspect that should be considered is the water model employed. There has been some discussion concerning which water model(s) to use in simulations of protein

solvation (Daggett and Levitt, 1993). In these studies we used the modified TIP3P model in CHARMM, which has been used in a number of other simulation studies (Roux and Karplus, 1991; Knapp and Muegge, 1993; Komeiji et al., 1993). Although the values of D, τ_1^{-1}, and τ_2^{-1} for a bulk TIP3P simulation do not agree exactly with the experimental values of these parameters (Table 3), the disagreement is not so great as to invalidate the current study. Furthermore, analyses in the current study have focused on comparisons of the dynamics of modified TIP3P in different environments, rather than on absolute values of dynamic properties. It seems unlikely that an alternative water model would radically transform the general patterns in dynamic behavior that have been observed.

During several simulations, restraints were imposed either on the protein and/or on the water molecules. In the case of inter-helix restraints on the protein atoms, simulation AN5, when repeated with such restraints present, yielded no significant differences from the results in the unrestrained AN5 simulations presented in this paper. Thus we can be reasonably confident that inter-helix restraints do not have artefactual effects on the dynamics of pore water. In some cases such restraints were necessary to maintain the integrity of the helix bundles. They are thought to mimic the effect of the lipid bilayer in stabilizing transmembrane helix bundle formation (cf. Chiu et al., 1991). In several simulations cylindrical restraints were imposed on the water molecules, to prevent their "evaporation" at the ends of the pore. It might be asked whether such restraints, acting primarily on waters in the cap zones, might not be responsible for the greater mobility of the water molecules in those regions. Two lines of argument suggest that this is not the case. First, simulations of water molecules in the presence of such restraints but in the absence of any protein do not increase the mobility of the cap waters. If the cavity generated by the restraints is of radius 6 Å or less, then the restraints tend to immobilize the water molecules somewhat (Sansom et al., 1996). However, this is not the case in the current simulations, where the radius of the cavity defined by the cylindrical restraints is greater than the van der Waals radius of the pore. The second, perhaps more persuasive, argument that cylindrical restraints do not result in an artefactual decrease in mobility comes from the studies on M2α7N5 in which, in the absence of such restraints, the same general pattern of water dynamic behavior is observed.

We have taken care to point out the relatively minor differences in dynamics protocol between the different simulations. This is important, as the observation of the same general pattern of water dynamic behavior despite such differences suggests that the exact conditions of the simulations do not greatly influence the overall result. Similarly, the observation of the same general pattern of dynamic behavior in several different models of transbilayer pores suggests that the overall result will prove robust to ongoing changes in the models as improved structural data emerge. Of course, this is not to imply that the details of dynamic behavior are insensitive to the details of the individual models, and thus are contingent upon the accuracy of the models.

Interpretation of results

Overall, our results confirm studies on gramicidin A (GA) (reviewed by Roux and Karplus, 1994) in demonstrating that water molecules confined within narrow transbilayer pores exhibit reduced mobility relative to bulk water. The current study extends the GA results in two respects: a) we have examined the dynamics of water in pores that are thought to more closely reflect the structure of ion channel proteins than does GA; and b) comparisons between different models enable us to dissect the factors influencing channel water dynamics.

The simulations of hydrophobic α-helix bundles and β-barrels reveal two effects contributing to water molecule immobilization within pores. Thus, in AN6 and BN8S8 the self-diffusion coefficients for the pore waters are almost the same, whereas the water dipole reorientation rates are significantly lower for the α-helix bundle model. This correlates with the preferential orientation of the water dipoles observed in AN5. This suggests that the reduction in translational mobility may be due to confinement of the waters, arising from their van der Waals interaction with the protein, whereas the additional reduction in rotational reorientation rates depends upon electrostatic interactions between the water dipoles and the pore. This view is reinforced by the results from those amphipathic helix bundles (δ-ToxN6 and M2α7N5) in which particularly strong electrostatic interactions are correlated with a marked reduction in rotational mobility of pore waters.

An unanticipated result from the AN5 and AN6 simulations is that they help to explain how parallel bundles of hydrophobic α-helices (e.g., Boc-(Ala-Aib-Ala-Aib-Ala)$_4$OMe, Menestrina et al., 1986; and phospholamban, Arkin et al., 1994, 1995; Adams et al., 1995) may form ion channels. Although the evidence for the existence of channels formed by hydrophobic helices is quite compelling, it is difficult to see how water molecules could stably occupy a pore without any polar pore-lining side chains. However, coupling of water dipoles to summated helix dipoles in a parallel helix bundle generates a favorable electrostatic interaction despite the absence of such polar side chains. Of course, to form a parallel helix bundle (which is necessary for such a water dipole/helix dipole interaction) requires that the helix dipole repulsions (in a low dielectric environment) be overcome. This may be achieved either by the interactions of peptide helices with an applied transbilayer voltage (in Boc-(Ala-Aib-Ala-Aib-Ala)$_4$OMe) (Menestrina et al., 1986) or possibly by interactions between non-bilayer regions of the polypeptide chain (e.g., in phospholamban; Arkin et al., 1995). Similar principles of helix/water interactions may apply in those regions of CFPs such as alamethicin that are predominantly hydrophobic.

Comparisons with other studies

Several different MD simulations of gramicidin A (Roux and Karplus, 1994) have revealed a single-file column of water molecules that forms a H-bonded chain within the GA channel. The self-diffusion coefficient of these waters is considerably lower than that of bulk water and a little lower than for the ion channel models considered in the current study. Using SPC water Chiu et al. (1991) estimated D = 0.06 $Å^2$ ps^{-1}; using modified TIP3P Roux and Karplus (1994) estimated D = 0.003 $Å^2$ ps^{-1}. The latter value is close to the experimental estimate of D = 0.004 $Å^2$ ps^{-1} for GA channel water. Thus, it is evident that substantial translational immobilization of water occurs within the GA pore. The conclusion of (Chiu et al., 1993) that GA channel water should be viewed as a distinct phase (not like a solid or a liquid or a liquid crystal) is relevant in this context. Furthermore, studies by Jordan and colleagues (Sancho et al., 1995) have emphasized that the presence of a cation within the GA channel will result in further reductions of the rotational mobility of intra-pore water.

Another model channel that has been used to simulate the dynamics of intra-pore water is that of Ghadiri and colleagues (Engels et al., 1995). This channel is formed by a stack of 10 β-sheet-like H-bonded cyclic peptides, with a channel running down the center of the peptide rings. The channel is wide enough to accommodate an alternating column of 1–2 waters. Estimation of the self-diffusion coefficient of the intra-pore TIP3P waters yielded D = 0.04 $Å^2$ ps^{-1}. This is close to the value obtained in simulation AN5, which has a pore of similar dimensions. Thus it appears that the reduced mobility of intra-pore water may be a general property of simple ion channels.

Comparisons may also be made with MD simulations of water confined within small volumes. Granick (1991) has provided an extensive review of studies of confined liquids, arriving at a general conclusion that relaxation times are prolonged by confinement in volumes of molecular dimensions. MD simulations of water molecules confined between two planar walls (Marchesi, 1983; Barabino et al., 1984) demonstrated a reduction in D and in τ_1^{-1} for waters adjacent to the wall. Simulations of modified TIP3P water confined within channel-like cavities (Sansom et al., 1996) suggest a degree of immobilization comparable to that observed in the current investigations. Thus confinement within a cylinder of radius 3 Å (cf. BN8S8) and length 60 Å resulted in a self-diffusion coefficient of D = 0.1 to 0.15 $Å^2$ ps^{-1}.

There have been many studies of the structure and dynamics of water molecules close to the surface of globular proteins. It is not our intention to provide a review of such work (see Teeter, 1991; Daggett and Levitt, 1993), but rather to highlight studies relevant to our results. Systems investigated include an alanine dipeptide (Rossky and Karplus, 1979), the active site of lysozyme (Brooks and Karplus, 1989), and bovine pancreatic trypsin inhibitor (Levitt and Sharon, 1988; Knapp and Muegge, 1993). All revealed a reduction of the mobility of surface water relative to bulk. A detailed study of the trp-holorepressor (Komeiji et al., 1993) suggested that D for surface water increased toward the bulk value as the distance of the water oxygen atom from the protein surface increased. Experimental estimates of D for surface water (e.g., Bellisent-Funel et al., 1992; Steinhoff et al., 1993) also suggest reduced translational mobility. The general picture emerging from such studies is that surface water is immobilized relative to bulk water such that $D_{SURFACE} \approx 0.25 D_{BULK}$. This should be compared with, e.g., $D_{PORE} \approx 0.16 D_{BULK}$ for channel model AN5. There have been fewer estimates of rotational reorientation rates of surface waters. For waters close to the hydrophobic regions of the Ala dipeptide (the most highly immobilized in this simulation), τ_1^{-1} and τ_2^{-1} were about one-third of their values for bulk water (Rossky and Karplus, 1979). This should be compared with, e.g., AN5, for which the values of τ_1^{-1} and τ_2^{-1} for intra-pore water are about an order of magnitude lower than those for bulk solvent.

Overall, such comparisons suggest that transbilayer pores contain extended columns of water whose dynamic properties are comparable to those of water bound to the surface of a globular protein. Comparison with studies of water held within small cavities suggests that much of this immobilization may be the result of confinement per se. Results for α-helix bundle models of channels indicate that a slightly greater degree of rotational immobilization may result from water/helix dipole interactions.

It is clear from our results that immobilization of intra-pore waters is not confined to single-file water such as that of GA but is present in much wider pores (e.g., BN8S8) and in pores lined with flexible polar side chains (e.g., M2α7N5). Thus immobilization appears to be a general property of water within ion channels. It will be important to confirm this by extending simulations to other systems (e.g., the pore domain of the nicotinic receptor, Sansom et al., 1995; and channels formed by de novo designed peptides, Lear et al., 1988). It will also be necessary to relate the extent of loss of rotational mobility to the decrease in local dielectric within such transbilayer pores. For example, Sancho et al. (1995) have suggested that within the GA/cation/water complex the dielectric of intra-pore water may be as low as ϵ = 5–10. To estimate ϵ for channel models may require long (~1 ns) MD simulations (e.g., model AN5) if approaches recently applied to estimation of ϵ for spherically confined water (Zhang et al., 1995) and for globular proteins (Smith et al., 1993; Simonson and Perahia, 1995) are to be employed. Careful attention to the treatment of long-range interactions will also be required if reliable estimates of ϵ are to be obtained. Preliminary simulations (Sansom, unpublished results) suggest that significant differences in ϵ of the intra-pore waters may occur between different channel models. In general, if ϵ can be estimated for the pore regions of ion channel models, then more realistic continuum electrostatics calculations upon channels should be possible, leading to greater insights into the nature of ion permeation and selectivity.

Our thanks to the Oxford Centre for Molecular Science for computational facilities. Our thanks to Peter Jordan (Brandeis) for his helpful comments and interest in this work.

This work was supported by grants from the Wellcome Trust. JB is an MRC research student.

REFERENCES

Adams, P. D., I. T. Arkin, D. M. Engelman, and A. T. Brünger. 1995. Computational searching and mutagenesis suggest a structure for the pentameric transmembrane domain of phospholamban. *Nature Struct. Biol.* 2:154–159.

Arkin, I. T., P. D. Adams, K. R. MacKenzie, M. A. Lemmon, A. T. Brünger, and D. M. Engelman. 1994. Structural organization of the pentameric transmembrane α-helices of phospholamban, a cardiac ion channel. *EMBO J.* 13:4757–4764.

Arkin, I. T., M. Rothman, C. F. C. Ludlam, S. Aimoto, D. M. Engelman, K. J. Rothschild, and S. O. Smith. 1995. Structural model of the phospholamban ion channel complex in phospholipid membranes. *J. Mol. Biol.* 248:824–834.

Barabino, G., C. Gavotti, and M. Marchesi. 1984. Molecular dynamics simulation of water near walls using an improved wall-water interaction potential. *Chem. Phys. Lett.* 104:478–484.

Bellisent-Funel, M. C., J. Teixeira, K. F. Bradley, and S. H. Chen. 1992. Dynamics of hydration water in protein. *J. Phys. I (France).* 2:995–1001.

Bertrand, D., J. L. Galzi, A. Devillers-Thiéry, S. Bertrand, and J. P. Changeux. 1993. Stratification of the channel domain in neurotransmitter receptors. *Curr. Opin. Cell Biol.* 5:688–693.

Bogusz, S., A. Boxer, and D. D. Busath. 1992. An SS1-SS2 β-barrel structure for the voltage-activated potassium channel. *Protein Eng.* 5:285–293.

Breed, J., and M. S. P. Sansom. 1994. Alamethicin channels modelled by simulated annealing and molecular dynamics. *Biochem. Soc. Trans.* 22:157S.

Brooks, B. R., R. E. Bruccoleri, B. D. Olafson, D. J. States, S. Swaminathan, and M. Karplus. 1983. CHARMM: a program for macromolecular energy, minimisation, and dynamics calculations. *J. Comp. Chem.* 4:187–217.

Brooks, C. L., and M. Karplus. 1989. Solvent effects on protein motion and protein effects on solvent motion. *J. Mol. Biol.* 208:159–181.

Brünger, A. T. 1992. X-PLOR Version 3.1. A System for X-ray Crystallography and NMR. Yale University Press, New Haven, CT.

Charnet, P., C. Labarca, R. J. Leonard, N. J. Vogelaar, L. Czyzyk, A. Gouin, N. Davidson, and H. A. Lester. 1990. An open-channel blocker interacts with adjacent turns of α-helices in the nicotinic acetylcholine receptor. *Neuron.* 2:87–95 .

Chiu, S. W., E. Jakobsson, S. Subramanian, and J. A. McCammon. 1991. Time-correlation analysis of simulated water motion in flexible and rigid gramicidin channels. *Biophys. J.* 60:273–285.

Chiu, S. W., J. A. Novotny, and E. Jakobsson. 1993. The nature of ion and water barrier crossings in a simulated ion channel. *Biophys. J.* 64: 98–109.

Cowan, S. W., T. Schirmer, G. Rummel, M. Steiert, R. Ghosh, R. A. Pauptit, J. N. Jansonius, and J. P. Rosenbusch. 1992. Crystal structures explain functional properties of two *E. coli* porins. *Nature.* 358:727–733.

Daggett, V., and M. Levitt. 1993. Realistic simulations of native-protein dynamics in solution and beyond. *Annu. Rev. Biophys. Biomol. Struct.* 22:353–380.

Dani, J. A., and D. G. Levitt. 1990. Diffusion and kinetic approaches to describe permeation in ionic channels. *J. Theor. Biol.* 146:289–301.

Eisenberg, D., and W. Kauzmann. 1969. The Structure and Properties of Water. Oxford, Oxford University Press.

Engel, A., T. Walz, and P. Agre. 1994. The aquaporin family of membrane water channels. *Curr. Opin. Struct. Biol.* 4:545–553.

Engels, M., D. Bashford, and M. R. Ghadiri. 1995. Structure and dynamics of self-assembling peptide nanotubes and the channel-mediated water organization and self-diffusion. A molecular dynamics study. *J. Am. Chem. Soc.* 117:9151–9158.

Esposito, G., J. A. Carver, J. Boyd, and I. D. Campbell. 1987. High resolution ^{1}H NMR study of the solution structure of alamethicin. *Biochemistry.* 26:1043–1050.

Fox, R. O., and F. M. Richards. 1982. A voltage-gated ion channel model inferred from the crystal structure of alamethicin at 1.5 Å resolution. *Nature.* 300:325–330.

Granick, S. 1991. Motions and relaxations of confined liquids. *Science.* 253:1374–1379.

Green, M. E., and J. Lewis. 1991. Monte Carlo simulation of the water in a channel with charges. *Biophys. J.* 59:419–426.

Gutman, M., Y. Tsfadia, A. Masad, and E. Nachiel. 1992. Quantitation of physical-chemical properties of the aqueous phase inside the phoE ionic channel. *Biochim. Biophys. Acta.* 1109:141–148.

Hille, B. 1992. Ionic Channels of Excitable Membranes, 2nd ed. Sinauer Associates, Sunderland, MA.

Jorgensen, W. L., J. Chandresekhar, J. D. Madura, R. W. Impey, and M. L. Klein. 1983. Comparison of simple potential functions for simulating liquid water. *J. Chem. Phys.* 79:926–935.

Karshikoff, A., V. Spassov, S. W. Cowan, R. Ladenstein, and T. Schirmer 1994. Electrostatic properties of two porin channels from *Escherichia coli. J. Mol. Biol.* 240:372–384.

Kerr, I. D., D. G. Doak, R. Sankararamakrishnan, J. Breed, and M. S. P. Sansom. 1996. Molecular modelling of Staphylococcal δ-toxin ion channels by restrained molecular dynamics. *Protein Eng.* 9:In press.

Kerr, I. D., J. Dufourcq, J. A. Rice, D. R. Fredkin, and M. S. P. Sansom. 1995. Ion channel formation by synthetic analogues of Staphylococcal δ-toxin. *Biochim. Biophys. Acta.* 1236:219–227.

Kerr, I. D., R. Sankararamakrishnan, O. S. Smart, and M. S. P. Sansom. 1994. Parallel helix bundles and ion channels: molecular modelling via simulated annealing and restrained molecular dynamics. *Biophys. J.* 67:1501–1515.

Knapp, E. W., and I. Muegge. 1993. Heterogeneous diffusion of water at protein surfaces: application to BPTI. *J. Phys. Chem.* 97: 11339–11343.

Komeiji, Y., M. Uebayasi, J. Someya, and I. Yamato. 1993. A molecular dynamics study of solvent behavior around a protein. *Proteins Struct. Funct. Genet.* 16:268–277.

Kraulis, P. J. 1991. MOLSCRIPT: a program to produce both detailed and schematic plots of protein structures. *J. Appl. Crystallogr.* 24:946–950.

Kreusch, A., and G. E. Schulz. 1994. Refined structure of the porin from *Rhodobacter blastica. J. Mol. Biol.* 243:891–905.

Lear, J. D., Z. R. Wasserman, and W. F. DeGrado. 1988. Synthetic amphiphilic peptide models for protein ion channels. *Science.* 240: 1177–1181.

Levitt, M., and R. Sharon. 1988. Accurate simulation of protein dynamics in solution. *Proc. Natl. Acad. Sci. USA.* 85:7557–7561.

Marchesi, M. 1983. Molecular dynamics simulation of liquid water between two walls. *Chem. Phys. Lett.* 97:224–230.

Mellor, I. R., D. H. Thomas, and M. S. P. Sansom. 1988. Properties of ion channels formed by *Staphylococcus aureus* δ-toxin. *Biochim. Biophys. Acta.* 942:280–294.

Menestrina, G., K. P. Voges, G. Jung, and G. Boheim. 1986. Voltage-dependent channel formation by rods of helical peptides. *J. Membr. Biol.* 93:111–132.

Montal, M. 1995. Design of molecular function: channels of communication. *Annu. Rev. Biophys. Biomol. Struct.* 24:31–57.

Oiki, S., V. Madison, and M. Montal. 1990. Bundles of amphipathic transmembrane α-helices as a structural motif for ion conducting channel proteins: studies on sodium channels and acetylcholine receptors. *Proteins Struct. Funct. Genet.* 8:226–236.

Oliver, A. E., and D. W. Deamer. 1994. α-Helical hydrophobic polypeptides form proton selective channels in lipid bialyers. *Biophys. J.* 66: 1364–1379.

Rahman, A., and F. H. Stillinger. 1971. Molecular dynamics study of liquid water. *J. Chem. Phys.* 55:3336–3359.

Rossky, P. J., and M. Karplus. 1979. Solvation. A molecular dynamics study of a dipeptide in water. *J. Am. Chem. Soc.* 101:1913–1936.

Roux, B., and M. Karplus. 1991. Ion transport in a model gramicidin channel: structure and thermodynamics. *Biophys. J.* 59:961–981.

Roux, B., and M. Karplus. 1994. Molecular dynamics simulations of the gramicidin channel. *Annu. Rev. Biophys. Biomol. Struct.* 23:731–761.

Sancho, M., M. B. Partenskii, V. Dorman, and P. C. Jordan. 1995. Extended dipolar chain model for ion channels: electrostriction effects and the translocational energy barrier. *Biophys. J.* 68:427–433.

Sankararamakrishnan, R., and M. S. P. Sansom. 1994. Kinked structures of isolated nicotinic receptor M2 helices: a molecular dynamics study. *Biopolymers.* 34:1647–1657.

Sankararamakrishnan, R., and M. S. P. Sansom. 1995a. Modelling packing interactions in parallel helix bundles: pentameric bundles of nicotinic receptor M2 helices. *Biochim. Biophys. Acta.* 1239: 122–132.

Sankararamakrishnan, R., and M. S. P. Sansom. 1995b. Water-mediated conformational transitions in nicotinic receptor M2 helix bundles: a molecular dynamics study. *FEBS Lett.* 377:377–382.

Sansom, M. S. P. 1991. The biophysics of peptide models of ion channels. *Prog. Biophys. Mol. Biol.* 55:139–236.

Sansom, M. S. P. 1993. Structure and function of channel-forming peptaibols. *Q. Rev. Biophys.* 26:365–421.

Sansom, M. S. P., and I. D. Kerr. 1995. Transbilayer pores formed by β-barrels: molecular modelling of pore structures and properties. *Biophys. J.* 69:1334–1343.

Sansom, M. S. P., I. D. Kerr, J. Breed, and R. Sankararamakrishnan. 1996. Water in channel-like cavities: structure and dynamics. *Biophys. J.* 70:693–702.

Sansom, M. S. P., R. Sankararamakrishnan, and I. D. Kerr. 1995. Modelling membrane proteins using structural restraints. *Nature Struct. Biol.* 2:624–631.

Schirmer, T., T. A. Keller, Y. F. Wang, and J. P. Rosenbusch. 1995. Structural basis for sugar translocation through maltoporin channels at 3.1 Å resolution. *Science.* 267:512–514.

Simonson, T., and D. Perahia. 1995. Internal and interfacial dielectric properties of cytochrome *c* from molecular dynamics in aqueous solution. *Proc. Natl. Acad. Sci. USA.* 92:1082–1086.

Smart, O. S., J. M. Goodfellow, and B. A. Wallace. 1993. The pore dimensions of gramicidin A. *Biophys. J.* 65:2455–2460.

Smith, P. E., R. M. Brunne, A. E. Mark, and W. F. van Gunsteren. 1993. Dielectric properties of trypsin inhibitor and lysozyme calculated from molecular dynamics simulations. *J. Phys. Chem.* 97:2009–2014.

Steinhoff, H. J., B. Kramm, G. Hess, C. Owerdieck, and A. Redhardtn. 1993. Rotational and translational water diffusion in the hemoglobin hydration shell: dielectric and proton nuclear relaxation measurements. *Biophys. J.* 65:1486–1495.

Tappin, M. J., A. Pastore, R. S. Norton, J. H. Freer, and I. D. Campbell. 1988. High resolution ^{1}H NMR study of the solution structure of δ-hemolysin. *Biochemistry.* 27:1643–1647.

Teeter, M. M. 1991. Water protein interactions: theory and experiment. *Annu. Rev. Biophys. Biophys. Chem.* 20:577–600.

Unwin, N. 1989. The structure of ion channels in membranes of excitable cells. *Neuron.* 3:665–676 .

Unwin, N. 1995. Acetylcholine receptor channel imaged in the open state. *Nature.* 373:37–43.

Zhang, L., H. T. Davis, D. M. Kroll, and H. S. White. 1995. Molecular dynamics simulations of water in a spherical cavity. *J. Phys. Chem.* 99:2878–2884.